Loss Identification using Inverse Thermal Modelling in Cage Induction Motor

Muhammad Kamran Razzaq

School of Electrical Engineering

Thesis submitted for examination for the degree of Master of Science in Technology.

Espoo 3.4.2019

Supervisor

Prof. Antero Arkkio

Advisor

Osemwinyen Osaruyi, M.Sc.

**Aalto University
School of Electrical
Engineering**

Author Muhammad Kamran Razzaq

Title Loss Identification using Inverse Thermal Modelling in Cage Induction Motor

Degree programme Automation and Electrical Engineering

Major Electrical Power and Energy Engineering   **Code of major** ELEC3024

Supervisor Prof. Antero Arkkio

Advisor Osemwinyen Osaruyi, M.Sc.

Date 3.4.2019   **Number of pages** 53+1   **Language** English

Abstract

Induction motors play a key role in moving the wheel of the modern industry with ever increasing demand and need of high performance and more efficient electric machines. To meet this ever increasing demand, this thesis covers the base of it i.e. losses occurring in the induction motor and thermal modelling of motor on the basis of the losses. In order to compute the iron losses, COMSOL Multiphysics has been put to use which is a very useful for vast analysis on the basis of Finite Element Analysis. A quasi 3D model of the induction motor is built in COMSOL to compute the losses occurring in the stator and rotor of the induction motor. These losses are then put to further application by building 3D thermal model of the same motor in COMSOL Multiphsics for modelling the thermal behaviour of the machine. In order to validate the theoretical work, experiments have been conducted on actual machine. In order to get vast practical data of temperature from the motor, a dedicated printed circuit board embedded with PT100 RTDs is designed to be put inside the stator of the machine while manufacturing. In the end, a detailed comparison of the simulated and measured results is done for deep understanding of the loss and thermal behaviour phenomena. The experimental results validated the thermal modelling for the simulated losses by showing strong coherence with the simulated results. The temperature rise data from sensors sheet inserted in the stator came out to be very useful in validating the results and in using the inverse thermal computation of losses.

Keywords Electric Machines, Iron loss, Copper Loss , Finite Element Analysis, Heat Transfer

Preface

The research work presented in this thesis work has been done in the Research Group of Electromechanics at Aalto University, School of Electrical Engineering, Finland between September,2018 and March, 2019.

I would like to express my deepest gratitude to Prof. Antero Arkkio for entrusting me with this work and giving his valuable support, guidance and support. It was an honour for me to work with him. I would also like to thank my adviser Terry and Ahmed for their continuous support, guidance and help throughout the work and the whole research group of Electromechanics for giving such a wonderful working and coordinating experience.

Finally, I would like to express my deepest gratitude and love to my family for their endless support, trust and encouragement throughout my life.

Espoo, 03.04.2019

Muhammad Kamran Razzaq

Contents

Symbols and abbreviations

Symbols

α	Temperature resistance coefficient
α_r	Radiation heat transfer coefficient
β	Absorptivity
κ	Transmitivity
ϵ_{thr}	Relative emissivity
η	Efficiency
σ	Specific conductivity
σ_{th}	Thermal conductivity
σ_{SB}	Stephan-Boltzman constant
χ	Susceptibility of material
μ_o	Permeability constant for air
ρ	Density
ϕ_{th}	Heat flow rate
Φ	Temperature difference
ω	Angular frequency in radian per second
Ψ	Flux Linkage
$\mathbf{A}$	Magnetic vector potential
B	Magnetic flux density
C_p	Specific heat capacity
f	Frequency
F	Bearing load
G	Electric conductance
G_{th}	Thermal conductance
D	Electric flux density
D_b	Inner diameter of bearing
E	electric field
h	Convective heat transfer coefficient
H	Magnetic flux intensity
I	Current (rms)
Je	Current density
k_R	Resistance factor
k_x	Thermal conductivity in x direction
k_y	Thermal conductivity in y direction
k_z	Thermal conductivity in z directionr
l_{av}	Average length of the turn
m	No. of phases
M	Magnetization
N	Number of turns
N_u	Nusselt number
p_{gen}	Generated power
P_{out}	Output power

P_{in}	Input power
P_{h}	Hysteresis loss
P_{e}	Eddy current loss
P_{ex}	Excess loss
P_{ρ}, b	Bearing friction loss
P_{cu}	Copper loss
P_{r}	Prandtl number
$P_{cu,s}$	Copper power loss in stator slots
$P_{cu,ew}$	Copper power loss in the endwinding
R	Resistance
R_{cv}	Convective heat transfer resistance
R_{e}	Reynold's number
S_{c}	Cross sectional area of conductor
R_{th}	Thermal resistance
T	Temperature
T_{amb}	Ambient temperature
V_{core}	Volume of the core
W_{h}	Energy density in core

Abbreviations

2D	Two Dimensional
3D	Three Dimensional
CFD	Computational Fluid Dynamics
EW	End Winding
FEA	Finite Element Analysis
FFT	Fast Fourier Transform
LPTN	Lumped Parameter Thermal Network

1 Introduction

1.1 Background

One of the most common type of motor running the wheel of world is Induction Motor. The simplicity in its rugged and economical construction, makes it suitable and reliable for a very large range of industrial and domestic applications. Induction Motor is free of any carbon brushes and commutators leading to lesser maintenance and is energized from the stator only getting output power from the rotor of the machine.

Being a very core part of rotating industrial wheels, it is of utmost importance to make them efficient to save up ever increasing demand and cost of power. In order to design and construct an efficient motor, it is very important to have deep knowledge of losses occurring in the machine. Loss in the induction motors can be classified as rotating, copper and iron loss. Stator of the motor comprises of thin laminated sheets of soft magnetic material having winding to produce rotating magnetic field. When current flows through the winding of the machine, I^2R occur due to resistance of the copper. Due to motion in the rotor of the machine, some energy in being lost due to friction in rotating parts i.e. bearings and lastly iron loss comprises of eddy current loss, hysteresis loss and excess loss.

Result of all these losses is the generation of heat in the motor. It is important to have prior knowledge of how much heat will be generated by these loss components since reliability of the machine heavily depends on it. There is some allowable temperature increase for each insulation class, which insulation of the motor winding can withstand. After this threshold, the deterioration rate of the insulation doubles after every 10 °C in temperature which can ultimately lead to the complete failure of insulation and hence the machine. This makes study of thermal modelling of electric machine of deep interest for the machine designers.

1.2   Thesis Objectives

The key objectives of thesis work are

- To identify and compute the iron loss in cage induction motor via finite element electromagnetic modelling.

- To build the thermal model of induction motor on the basis of loss computed from electromagnetic model and compute temperature rise in the motor.

- To design temperature measurement setup from machine i.e. PT100 sensors sheet to be inserted inside stator for finding precise temperature rise in machine core and end winding.

- Inverse thermal modelling for the computation of machine loss from the temperature rise in the actual machine.

1.3   Thesis Structure

Following is the breakdown of the structure of the thesis work

- **Chapter 2**: In chapter 2, the background theory and literature review is done about the electromagnetic loss in the electric machines, modelling and computation of loss and thermal modelling of the machine through various techniques.

- **Chapter 3**: In this chapter, the methodology for the modelling cage induction motor in COMSOL Multiphysics for the computation of iron losses. Also it explains how the thermal model is being built in the COMSOL on the basis of loss computed in electromagnetic model.

- **Chapter 4**: In chapter 4, the measurement set up used in the experimentation is explained and a detailed comparison of the simulated results and the measured results in presented.

- **Chapter 5**: In the final chapter, the concluding remarks about the whole thesis work are added with future perspective of this work for the further research purpose.

2 Losses and their Thermal Modelling

2.1 Losses in Electric Machines

The difference between input power to the machine and the corresponding output power determines how much power we have lost during this energy conversion process giving out the efficiency of any machine.

$$\eta = \frac{P_{\text{out}}}{P_{\text{in}}} = \frac{P_{\text{out}}}{P_{\text{out}} + P_{\text{loss}}} \tag{2.1}$$

For example in induction motor, 3 phase *AC* electric power is being fed to the stator winding of the machine to produce rotating magnetic field. This rotating flux induces voltage in both stator and rotor windings. Current is induced in the rotor bars in accordance to Farady's Law which interacts with the revolving flux to produce torque resulting in rotor rotation. During this whole energy conversion process, the energy lost can be categorized as following.

- Rotational loss

- Copper loss

- Iron loss

2.1.1 Rotational Losses

Losses occurring due to friction in rotating parts of the machine such as rotor bearings, windage loss of the rotor. These losses mainly depend upon the speed of motor, type of bearing being used and its lubrication and loading of the machine. Bearing friction losses according to SKF can be calculated as following [1]

$$P_{\rho,\text{b}} = 0.5\Omega\mu F D_{\text{b}} \tag{2.2}$$

where Ω is the angular frequency of the shaft supported by the bearing, μ is the friction coefficient (typically 0.08-0.2 for steel-on steel sliding contact surface combination), F is the bearing load and D_{b} is the inner diameter of the bearing. Windage losses on the other hand become more prominent as the speed of machine is increased. These losses result due to friction between the rotating surfaces and the surrounding gas i.e. air.

2.1.2 Copper Losses

Copper losses, also referred as resistive losses, occur in the winding of the machine and can be calculated as follows [1]

$$P_{\text{cu}} = mI^2 R_{\text{AC}} \tag{2.3}$$

where m is the number of phases, I is current and R_{AC} is the AC resistance of the phase winding. The AC resistance can be obtained using equation below

$$R_{\text{AC}} = k_R (N l_{\text{av}})/(\sigma S_{\text{c}}) \tag{2.4}$$

where k_R is the resistance factor, N is the number of turns, l_{av} is the average length of a turn, S_c is the cross sectional area of the conductor and σ is specific conductivity of the winding conductor.

The temperature rise calculation in winding occurring due to copper losses, can be divided into losses occurring in the end winding and resistive loss occurring in the conductor present inside the slots of the machine. For the efficiency calculation of the machine, DC resistance of the winding is used to calculate the resistive loss part and skin effect is taken into account in additional losses of the machine.

2.1.3 Iron Losses

The core of the electrical machine is composed of ferromagnetic materials which are made by thin laminated sheets and stacked to form a compact assembly. In these magnetic materials, there exists elementary magnets, Weiss domains, separated from each other by domain walls also known as Bloch walls. When an external magnetic field is applied to these materials, it makes the domain walls to move providing the net magnetization of the material. This relation can be described by the material susceptibility i.e.

$$M = \chi H \tag{2.5}$$

where χ is the susceptibility of the material, H is the magnetic flux intensity and M is the magnetization. So the magnetic flux density of the material is enhanced from its value in the air due to this magnetization property of the material.

$$B = \mu_o(H + M) \tag{2.6}$$

and we can describe total magnetic flux density B with a material coefficient called permeability μ

$$B = \mu H \tag{2.7}$$

When the stator core of the machine is subjected to some external field (by connecting stator winding with 3 phase AC source), rotating magnetic field is produce which varies its direction in time. When external magnetic field intensity H is increased in one direction, the flux density B in magnetic material also increases in same direction as shown in the 2.3 until it reaches its saturation limit. After that, a very large increase in H will result in very small change in B.

When the direction of the H is changed, B also start to change its direction but it lags behind H such that when H becomes zero, there remains some flux density called remnant flux density B_r. Some negative value of H is required to completely make flux density in material equal to zero referred as coercive magnetic intensity H_c. A loop is formed between B and H due to this phenomenon known as Hysteresis loop as shown in Fig. 2.3. In order to magnetize the core of machine, some energy is being transferred from source to the magnetic core of the machine to set up the magnetization during one interval. However, energy returned to the source in other interval is less than energy inflow. Hence there is net flow of energy from source to core. This energy loss goes to heat up the core. This loss of power occurring due to
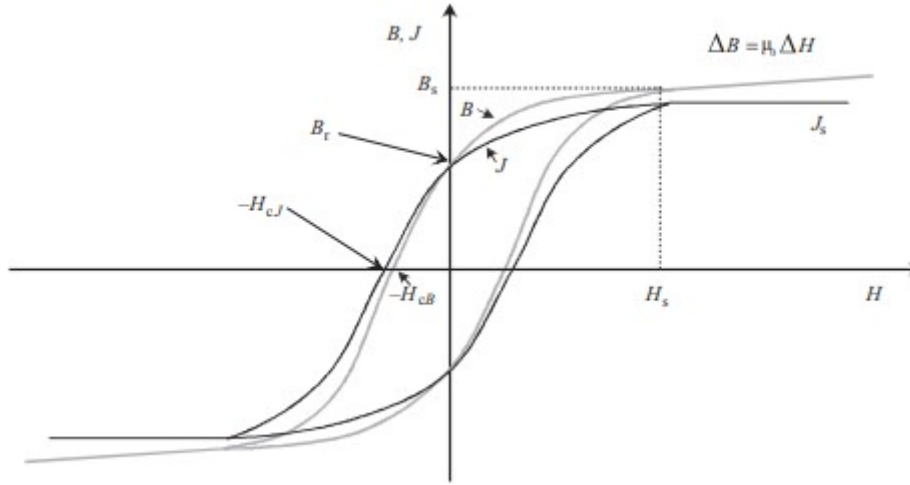
Figure 2.1: BH loop of soft magnetic material

hysteresis effect is called hysteresis loss and is directly proportional to the area of B-H loop [2]

$$P_{\mathrm{h}} = V_{\mathrm{core}} W_{\mathrm{h}} f \tag{2.8}$$

where V_{core} is the volume of the core, f is frequency and W_{h} is the energy density in the core and is equal to $\oint H dB$ (area of the B-H loop). Due to multi-valued non-linear characteristics of the B-H curve, it is not very simple to compute above expressions. Different models have been developed to study hysteresis in magnetic materials such as Jiles-Atherton model [3], taking into account physical parameters of the isotropic magnetic materials, Preisach model of hysteresis [4] but a common relation to calculate the hysteresis loss, developed by Charles Steinmetz, after number of experimentation, is

$$P_{\mathrm{h}} = K B_{\mathrm{max}}^{n} \tag{2.9}$$

which is also equal to the area of B-H loop, where K is constant, n varies from $1.5 - 2.5$ and B_{max} is the maximum flux density. Hence from above equations, hysteresis power loss can be calculated as

$$P_{\mathrm{h}} = K_{\mathrm{h}} B_{\mathrm{max}}^{n} f \tag{2.10}$$

where K_{h} is constant and its value depends on the magnetic material and core volume. Since the flux is alternating in the core of the magnetic material, then as per Faraday's law of electromagnetic induction, voltage is induced in the core. Since magnetic materials are not 100% insulators and have some conductivity, a current starts to flow due to induced voltages resulting in $I^2 R$ losses in the core. These currents are called eddy currents and losses occurred due to eddy current are termed as Eddy current losses. To reduce them, resistivity of the core material is usually increased by adding some impurities (Silicon, 4%) and instead of using one solid core, thin laminated sheets of magnetic materials insulated from each other are used to make

the core of the machine. Eddy currents losses can be computed by the following relation

$$P_{\text{e}} = K_{\text{e}} B_{\text{max}}^2 f^2 \tag{2.11}$$

where K_{e} is a constant and its value depends on material and thickness of lamination. However this classical separation of iron losses studied by C.D. Graham [5] deviates from the fact that total dynamic iron losses measured are not equal to the sum of eddy current and hysteresis loss. This gave rise to another loss type called excess losses, studied by Giorgio Bertotti [6] The total iron loss of the machine can be expressed as

$$P_{\text{Fe,total}} = P_{\text{h}} + P_{\text{e}} + P_{\text{ex}} \tag{2.12}$$

$$P_{\text{Fe,total}} = K_{\text{h}} B_{\text{max}}^n f + K_{\text{h}} B_{\text{max}}^2 f^2 + K_{\text{ex}} B_{\text{max}}^{1.5} f^{1.5} \tag{2.13}$$

The Electromagnetic modelling of the induction machine for computation of parameters and losses has vastly been done using different approaches and FEA tools such as $FEMM$, $COMSOL$ etc. In [7], a quasi 3D model of the Induction motor has been built in $COMSOL$ which requires precise layout of motor geometry and accurate material properties. The electromagnetic field of the motor is solved by using Maxwell's equation combined with material equations and properties in the rotating machinery physics of $COMSOL$.

$$\sigma \frac{\partial \boldsymbol{A}}{\partial t} + \boldsymbol{\nabla} \times \boldsymbol{H} - \sigma \boldsymbol{v} \times \boldsymbol{B} = \boldsymbol{J}_{\text{e}} \tag{2.14}$$

$$\boldsymbol{\nabla} \times \boldsymbol{A} = \boldsymbol{B} \tag{2.15}$$

where B is magnetic flux density, H is magnetic field intensity, $\boldsymbol{v}$ is velocity of conductors, $\boldsymbol{A}$ is magnetic vector potential and J_{e} is externally generated current density. The model has been solved by setting up external circuit equation for energizing the coils of winding with 3 phase balanced sinusoidal voltage source. The mesh with free triangular elements was set in domains of geometry to solve the model in steady state. The final values of parameters such as speed, torque, current calculated from simulation gave quite accurate values when compared to motor's catalogue value proving the significance and accuracy of FEA methods and tools in precise modelling of the machine. In [8] , motor parameters have been computed using finite element analysis in FEMM.

Further FEA analysis has been put into calculating the losses in induction motor in [9] since in traditional motor design, iron losses are computed on basis of average magnetic circuit model in combination with empirical formula and coefficient to modify the results, which are not in complete coherence with the measurement results [10]. In this, iron and stray losses are calculated using field circuit coupled with time-stepping finite element method based on Bertotti iron loss separation model. The iron losses are computed by taking into account both alternating and rotating magnetization in the core [11]. However, some assumptions were taken for formulating the model such as effect of displacement current was ignored, all field

quantities were changing sinusoidally and skin effect was ignored assuming uniform current density in the winding section.

2.2   Heat Transfer

All the losses occurring in the machine result in the generation of heat. Heat generated in different parts of the machine transfers within the machine and to the environment on the basis of temperature gradient i.e. from high temperature region to lower temperature region. This heat removal mechanism is of particular importance in the reliable operation of electrical machine as it is important to keep the insulation and winding temperature below their thermal limit. As the temperature rise higher than rated thermal limit of machine drastically reduce its life. Heat gets transferred via conduction, convection or radiation from area of high energy potential to lower.

2.2.1   Conduction

In conduction, heat is being transferred by the molecular interaction of material with each other. Molecules with high energy content impart their energy to neighbouring molecules and this process continues throughout the material from a region of high energy or high temperature to a region of lower energy or temperature via lettuce vibrations. This kind of transfer is possible in all three matter states i.e. solid, liquids and gasses. The transfer mechanism is also carried out in metals which have free electrons and the ability of metal to transfer heat depends upon the number of free electrons.

This phenomenon was studied by J. Fourier giving the Fourier's law in his remarkable publication *Theorie Analytique de la Chaleur* in 1882. It states that heat transfer rate is directly proportional to the heat transfer cross sectional area, temperature gradient and material property to conduct the heat i.e.

$$\varphi_{\text{th}} = -\lambda S \nabla T \tag{2.16}$$

where φ_{th} is flow rate of heat, S is the cross sectional area for heat transfer, ∇T is gradient of temperature and λ is the thermal conductivity of the material $[W/mK]$. The negative sign shows that heat transfers from region of high temperature to lower temperature. Thermal conductivity of the material depends on the temperature as well since thermal conductivity of metals decreases with increase in temperature whereas it reduces in insulators with temperature rise. The differential equation governing the conduction with in some volume having heat generation source can be written as [12]

$$p_{th} = \rho C \frac{\partial T}{\partial t} + \nabla T \tag{2.17}$$

where p_{th} is the power density, ρ is the density of material $[kg/m^3]$, C is the specific heat capacity $[W/kgK]$. Every material bears some resistance to flow of heat termed as thermal resistance R_{th} and an analogy can be made between electrical resistance and thermal resistance. Electrical resistance is the ratio of potential difference to the

current flowing through conductor, in the same way, thermal resistance is basically ratio of temperature difference to rate of flow of heat, φ_{th} through the material.

$$R_{\text{th}} = \frac{\Theta}{\varphi_{\text{th}}} = \frac{l}{\lambda S} \tag{2.18}$$

where Θ is the temperature difference, l is the length of material, S is the surface area and λ is the thermal conductivity. The unit of thermal resistance is $[K/W]$.

2.2.2 Convection

Convective heat transfer is defined as the transfer of heat from high temperature region (usually a solid surface) to a region of lower temperature (fluids) as a result of actual movement of the molecules of fluids. This mode of energy transfer occurs due to bulk (macroscopic) movement of the fluid particles due to presence of temperature gradient, thus resulting in heat transfer. Heat transfer in fluid occurs simultaneously by conduction (via random molecular vibration), also known as heat diffusion, and via bulk movement of fluid particles (advection). This rate of energy transfer depends upon density of fluid and temperature difference. According to Newton's law of cooling,

$$q_{\text{c}} = \alpha \left(T_{\text{s}} - T_{\text{amb}} \right) \tag{2.19}$$

where q_{c} is the convective heat flow rate $[W/m^2]$, α is the convective heat transfer coefficient $[W/m^2 K]$, T_{s} is the temperature of the surface exposed for convection $[K]$ and T_{amb} is the ambient temperature $[K]$. Convection heat transfer coefficient depends on the conditions in the boundary layer, which is further dependent on the geometry of surface, fluid motion nature as an assortment of fluid thermodynamic and transport properties [13]. The resistance to convective heat transfer is termed as thermal convection R_{cv} resistance and is equal to

$$R_{\text{cv}} = \frac{1}{\alpha S} \tag{2.20}$$

where S is surface area of solid in contact with fluid. In order to make convection heat transfer problem evaluation simple and keep the number of parameters simple in solution, various dimensionless parameters have been generated. Out of many of them, Nusselt number N_{u}, Reynolds number R_{e} and Prandtl number P_{r} are of key importance when calculating heat transfer from solid surfaces to the coolant fluid. Nusselt number can be used to describe convection heat transfer coefficient as

$$N_{\text{u}} = \frac{\alpha L}{\lambda} \tag{2.21}$$

where L is the characteristic surface length and λ is thermal conductivity of the coolant. The effectiveness of the convection heat transfer coefficient can be measured as compared to conduction heat transfer.

Reynold's number can be defined as the ratio between inertia and viscous force i.e.

$$R_{\text{e}} = \frac{vL}{v} \tag{2.22}$$

where v is the coolant speed on the surface, L is the characteristic length of the surface and v is the kinematic viscosity of the coolant. The value of Reynold's number at which flow becomes turbulent is called critical Reynold's number. For tubes the characteristic length is defined as

$$L = \frac{4S}{l_{\mathrm{p}}} \tag{2.23}$$

where S is the cross sectional area of the tube and l_{p} is the wetted perimeter of the tube.

Prandtl number describes the relation between momentum and thermal diffusivity. It's the thickness ratio of the velocity and thermal boundary layers.

$$P_{\mathrm{r}} = \frac{C_{\mathrm{p}}\mu}{\lambda} \tag{2.24}$$

where C_{p} is the specific heat capacity, μ is the dynamic viscosity and λ is thermal conductivity of the coolant.

Further the convection heat transfer can be classified as per nature of the flow. If we enforce the flow rate to increase via some external source such as fans, pumps etc., this is called forced convection. On the other hand, if convection is occurring freely without any influence of external means, then it is termed as natural convection. In natural convection, the flow of fluid takes place majorly because of density difference of fluids due to temperature variations [13].

2.2.3 Radiation

The third type of heat transfer is via radiation as different bodies emit electromagnetic radiations depending upon their energy content. These electromagnetic radiations cover the entire spectrum of wavelengths such as ultraviolet, visible, infrared radiations etc. These electromagnetic radiations are independent of medium meaning they can travel from vacuum, opposite to conduction and convection which require some medium for their transmission. The ability of a body to absorb radiation is called absorptivity β, energy reflected back by body defines its reflectivity η and energy transmitted through it is called transmissivity κ . The sum of all these parameters is equal to 1.

$$\beta + \eta + \kappa = 1 \tag{2.25}$$

So, heat flow rate because of radiation can be explained by the Stephan-Boltzmann law.

$$q_{\mathrm{th}} = \frac{\Phi_{\mathrm{th}}}{S} = \varepsilon_{\mathrm{thr}}\sigma_{\mathrm{SB}}\left(T_1^4 - T_2^4\right) \tag{2.26}$$

where T_1 is the thermodynamic temperature of the radiating surface, T_2 is the thermodynamic temperature of the absorbing surface, σ_{SB} is Stephan-Boltzmann constant and its value is 5.67×10^{-8} $[W/m^2 K^4]$. $\varepsilon_{\mathrm{thr}}$ is the relative emissivity between the absorbing and emitting surface and its value is highly dependent on surface characteristics and position. Emissivity of the ideal black body is equal to one and

emissivity of all other bodies is measured in relative comparison to black body. The relative emissivity between a grey painted electrical machine and its surrounding is about 0.85.

There also exists thermal resistance of radiation, in analogy to conduction and convection thermal resistance and is defined as

$$R_{\text{th}} = \frac{T_1 - T_2}{\Phi_{\text{th}}} = \frac{T_1 - T_2}{\varepsilon_{\text{th}}\sigma_{\text{SB}}\left(T_1^4 - T_2^4\right)} = \frac{1}{\alpha_{\text{r}}S} \tag{2.27}$$

where

$$\alpha_{\text{r}} = \varepsilon_{\text{th}}\sigma_{\text{SB}}\frac{T_1^4 - T_2^4}{T_1 - T_2} \tag{2.28}$$

α_{r} is the heat transfer coefficient of the radiation and its value depends on the temperature of the absorbing and emitting surfaces.

2.3 Thermal Modelling of Electric Machines

The understanding of thermal behaviour of the electric machines is of key importance for the reliable operational design since all the losses occurring in machine are due to motion, flux, currents and hysteresis result in the form of temperature rise in different parts of the machine. Thermal modelling in electric machines is basically mathematical prediction of this temperature rise as a result of losses and an accurate determination of it is very important. The flow of heat in machine has a strong analogy with the flow of the electric current and those analogous thermal quantities can be compared as following.

Table 2.1: Analogy between Thermal and Electric Flow Parameters

Thermal Flow	Symbol	Unit	Electric Flow	Symbol	Unit
Heat Quantity	Q_{th}	J	Electric Charge	Q	C
Heat Flow rate	Φ_{th}	W	Electric Current	I	A
Heat Flow Density	q_{th}	W/m^2	Current Density	J	A/m^2
Temperature	T	K	Electric Potential	V	V
Temperature rise	Θ	K	Voltage	V	V
Thermal Conductivity	λ	W/mK	Electric Conductivity	σ	S/m
Thermal Resistance	R_{th}	K/W	Electric Resistance	R	Ω
Thermal Conductance	G_{th}	W/K	Electric Conductance	G	S
Heat Capacity	C_{th}	J/K	Capacitance	C	F

In order to calculate the temperature, different models have been adopted such as

- Lumped Parameter Thermal Model

- Thermal Analysis using Finite Element Analysis (FEA)

2.3.1 Lumped Parameter Thermal Model

One of the most popular method for the estimation of temperature rise in electrical machines is lumped parameter thermal model. It is based on geometric division of electric system into number of lumped components which define the thermal resistance, capacitance and heat sources which are interconnected to each other to make a mesh. The values to these lumped parameters depends upon the dimensions of the components and their thermal properties. This model can be used for both transient and steady state analysis

In order to understand its basics, consider a 1-D thermal network for heat flow in a block of length l, cross sectional area of A, temperatures on its two ends be T_1 and T_2. The heat generated inside the solid block can be represented as a current source P_{losses}. Equivalent lumped thermal model of the block can be represented as [14]
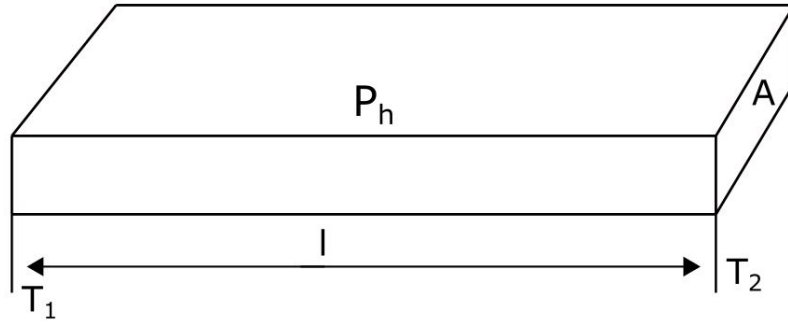
Figure 2.2: Heat flow in block
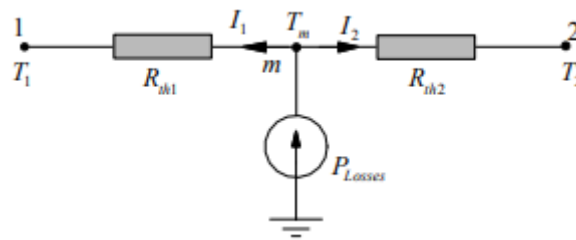
Figure 2.3: Lumped Thermal Network

The thermal node is taken to be in the mid-point of the block, the block offers the thermal resistance to the heat source from its end points and this thermal resistance can be computed as $R_{th1} = R_{th2} = \frac{l/2}{\lambda A}$

where λ is the thermal conductivity of the block material. The figure shows the heat transfer from the source node 'm' to the end nodes through the thermal resistance of the material.

However in actual machine, this network is somewhat more complex as heat generated in different parts of machine transfers in all direction and geometry of heat generation area is also complicated. Some assumptions are made in making the lumped thermal model of induction machines [15].

- The flow of heat in radial and axial direction of machine is independent.

- A single mean temperature defines heat flow in radial and axial direction.

- Circumferential heat flow in not taken into account.

The lumped parameter thermal modelling is an ideal tool for the optimization and parametric studies of different configuration of motors because of lesser number of nodes. In lumped parameter thermal modelling, parameter identification of the $LPTN$ model is very important and [16] has put two deterministic methods, Gauss-Newton and Levenberg-Marquardt, and one stochastic method, Genetic algorithm, to use in order to identify the unknown influent parameters of lumped parameter thermal model of the machine.

2.3.2 Thermal Analysis using Finite Element Approach (FEA)

Finite Element Analysis for the investigation of thermal behaviour of machine is another very useful tool which can be used for both 2D and 3D analysis instead of making lumped parameters of the machine. Different FEA tools such as COMSOL, FEMM, ANSYS etc. are equipped with thermal analysis tool using FEA. These tools are specifically very useful in thermal analysis of complex geometries with accurate and detailed information of temperature in different parts of the machine. 2D [17] and 3D [18] [19] [20] thermal models of electric machines have been studied previously for the computation of loss and temperature distribution. In 3D finite element thermal modelling, following heat equation has been implemented for temperature evaluation

$$\frac{\partial}{\partial x}\left(k_x \frac{\partial T}{\partial x}\right) + \frac{\partial}{\partial y}\left(k_y \frac{\partial T}{\partial y}\right) + \frac{\partial}{\partial z}\left(k_z \frac{\partial T}{\partial z}\right) + q \quad = \quad \rho C_{\text{p}} \frac{\partial T}{\partial x} \tag{2.29}$$

where k_x, k_y, k_z are the thermal conductivities in x, y and z direction respectively and q is the heat generated in the machine due to losses. This q can be inserted in to model after by the electromagnetic model for computation of loss for forward thermal modelling of the machine. Similarly the winding in the machine can be modelled by their heat source as I^2R losses knowing the current and resistance of the winding. It is important to apply appropriate convective boundaries for surfaces having contact with outside air.

Since finite element modelling is computationally expensive and it becomes more time consuming when we make 3D analysis. In such cases, it is very convenient to use the symmetry of the machine for making models for example a 4 pole machine can be modelled for only $1/4th$ of its geometry (per pole) and applying appropriate

periodic and anti-periodic boundary conditions gives desirable results in much lesser time.

In addition of FEA thermal modelling, computational fluid dynamics (CFD) modelling of electric machines can also be done for determining the temperature distribution. In [21], thermal optimization of HSPM (High Speed Permanent Magnet) machine has been done by computing losses in 2D time stepping FEA and substituting them in CFD model to estimate the temperature distribution of the machine.

2.3.3   Inverse Thermal Modelling

Inverse modelling concept is based on the estimating the unknown parameters from the measurement of the observable system parameters. This technique has evolved recently from theoretical research problem to a practical engineering tool. Inverse problem can be solved either as a parameter estimation or as a function estimation approach [22].

In the aforementioned thermal models, we need to have complete and exact knowledge of machine parameters and thermal properties such as thermal conductivities, losses, magnetic material properties to predict the temperature of machine. This type of modelling is referred as forward modelling. The result of all losses in machine occur in the form of temperature rise which gives us a solid ground to take this observable quantity and use it in inverse modelling of machine for prediction of origin of this temperature rise i.e. power losses. Hence instead of directly measuring losses occurring in machine, measuring temperature rise in different accessible points can give us fairly accurate estimation of losses occurring in machine.

The principle of the method lies in the fact that when a unit function of heat source is applied to a medium in the steady state, the instantaneous temperature rise rate is directly proportional that heat generation on that point. So, a temperature versus time curve is plot at that point, the slope of the curve at the instant of applying heat function gives the measure of generation of heat at that point.

This has been applied to loss estimation of magnetic material in [23] by using copper-constantan thermocouples installed on machine core to measure the temperature rise occurring due to losses. Over 300 of these thermocouples were installed in the core of an $80MW$ water wheel alternator to get the temperature rise curve to estimate the losses with fair accuracy of 5% error. A similar approach used in [24] for the identification of local iron loss using inverse thermal modelling approach. The general heat diffusion equation can be expressed as [25]

$$\frac{\partial \vartheta}{\partial t} = a\nabla^2\vartheta + \frac{p_{\text{gen}}}{c_{\text{th}}\,\gamma} \qquad (2.30)$$

with the thermal diffusivity

$$a = \frac{\sigma_{\text{th}}}{c_{\text{th}}\,\gamma} \qquad (2.31)$$

where c_{th} is the specific thermal capacity $[J/kgK]$, γ is the material density in $[kg/m^3]$, σ_{th} is the thermal conductivity W/mK, p_{gen} is the power density in $[W/m^3]$

and θ is the temperature $[K]$. When the power generation inside investigating volume is change instantly, it can be assumed that heat transfer during that small time is negligible and heat generated can be calculated by simplifying above equation as

$$p_{\text{gen}} = c_{\text{th}} \, \gamma \left(\frac{d\vartheta}{dt} \right)_{t \to 0^+} \tag{2.32}$$

Using above principle as the base of inverse thermal modelling, firstly a FEM simulation model of the investigated machine to find the losses was done to be inserted in 3D FEM thermal model of machine as the forward model to compare with measurement data. In order to measure the temperature rise at different points at machine, $PT100$ thermal sensors and a thermal infrared camera. The results show quite good agreement with the simulated temperature rise curves at that point assuming a that all external conditions, such as cooling remain unchanged during the initial phase preceding the change in losses.

In addition to loss identification in electric machines, inverse thermal model is useful tool for correctly estimating the thermal parameters of the machine as the measured thermal behaviour of the machine can differ significantly from the simulated models. These inaccuracies may occur due to complex anisotropic conductivity and thermal contact resistances [26] [27] , effect of radiation thermal resistance [28] and high impact of process parameters [29] . Hendtic et al. [30], applied inverse thermal modelling approach to identify the accurate thermal parameters of the model with the help of parametric model order reduction for efficient calculation effort.

3   Electromagnetic and Thermal Modelling

This chapter explains the formulation of electromagnetic and heat transfer model for the targeted electrical machine. Firstly, a 2D electromagnetic model of the stator core of a 37kW induction motor with blocked rotor without copper bars is developed using COMSOL Multiphysics. In the second section, core losses estimated from the electromagnetic model are directly coupled in the thermal model as heat sources to solve the temperature distribution on the stator and rotor of the machine.

3.1   Finite Element Modelling using COMSOL

Finite Element Method is a numerical method for the computation of different complex engineering problem and has a vast range of application such as in solving electromagnetic problems, heat transfer, fluid dynamics, structural analysis etc. The main idea of this approach is dividing the problem domain in to small non-overlapping elements, called finite elements. The simple elements are modelled with a set of partial differential equations and assembled for the whole geometry of domains to solve the entire problem. The subdivision of the domains into smaller elements gives the advantage of accurately representing a complex geometry, segregate domains on the basis of their material properties and include local effects.

The fundamentals of electromagnetic field problems in space and time are governed by the set of Maxwell's equations and material equation. These equations give basis for solution of magnetic fields problems by explaining Ampere's law, Gauss's Law and Faraday's Law and are summarized as following

$$\boldsymbol{\nabla}.\boldsymbol{D} \quad = \quad \rho \tag{3.1}$$

$$\boldsymbol{\nabla}.\boldsymbol{B} \quad = \quad 0 \tag{3.2}$$

$$\boldsymbol{\nabla} \times \boldsymbol{E} \quad = \quad -\frac{\partial \boldsymbol{B}}{\partial t} \tag{3.3}$$

$$\boldsymbol{\nabla} \times \boldsymbol{H} \quad = \quad \boldsymbol{J} + \frac{\partial \boldsymbol{D}}{\partial t} \tag{3.4}$$

and material equations

$$\boldsymbol{D} \quad = \quad \varepsilon \boldsymbol{E} \tag{3.5}$$

$$\boldsymbol{J} \quad = \quad \sigma \boldsymbol{E} \tag{3.6}$$

$$\boldsymbol{B} \quad = \quad \mu \boldsymbol{H} \tag{3.7}$$

In addition to above mentioned set of equations, we need to define boundary conditions in our problem domain to find the solution. These boundaries can be the borders

between problem domain and the outer environment or the interfaces within the problem domain due to different material properties. Following are the basic boundary conditions which need to be taken into account while solving the problem via FEA.

- Dirichlet boundary condition in which $\boldsymbol{A}$ (magnetic vector potential), is constant or field is paralled to the boundary

- Homogeneous Neumann boundary condition in which field is perpendicular to the boundary i.e. $v\frac{\partial \boldsymbol{A}}{\partial \boldsymbol{n}} = 0$

- (Anti)periodic boundary is used when we have symmetric sectors in our problem domain and at the interface boundaries $A_1 = \pm A_2$ satisfies.

In order to apply aforementiond finite element analysis on the motor under consideration, COMSOL Multiphysics software has been used. The parameters of the induction motor design used in the simulation are shown in the Table3.1. The detailed explanation of the COMSOL model used will be given in the subsequent section.

Table 3.1: Motor Parameters

Sr. No	Parameter	Value
1	Rated Power	$37kW$
2	Rated Voltage	$400V$
3	Poles	4
4	Frequency	$50Hz$
5	Conductors in stator slots	12
6	Layers of stator winding	1
7	No. of stator slots	48
8	Effective length of stator	$0.249m$
9	Stator outer diameter	$0.310m$
10	Stator inner diameter	$0.2m$
11	Air gap	$0.8mm$
12	Winding resistance/phase	0.075Ω
13	End winding reactance/phase (50Hz)	0.092Ω

As per geometric dimensions and parameters of the motor, the geometry of the machine is drawn. Since there are 4 poles in the stator with 48 slots, there will be 4 slots per pole per phase of the machine. Motor has 3 phase distributed winding having coil pitch in slot pitches equal to 12, so instead of simulating whole geometry, only one pole sector of motor is enough to analyze the motor which will greatly reduce the computation time for obtaining the solution as shown in the Fig 3.1. The stator of the 37kW induction motor has been used for providing rotating magnetic field by connecting the winding with 3 phase sinusoidal input and aim of the work is to compute iron losses, there is no motion required for the rotor. That's why there are no slots for rotor bars or winding.
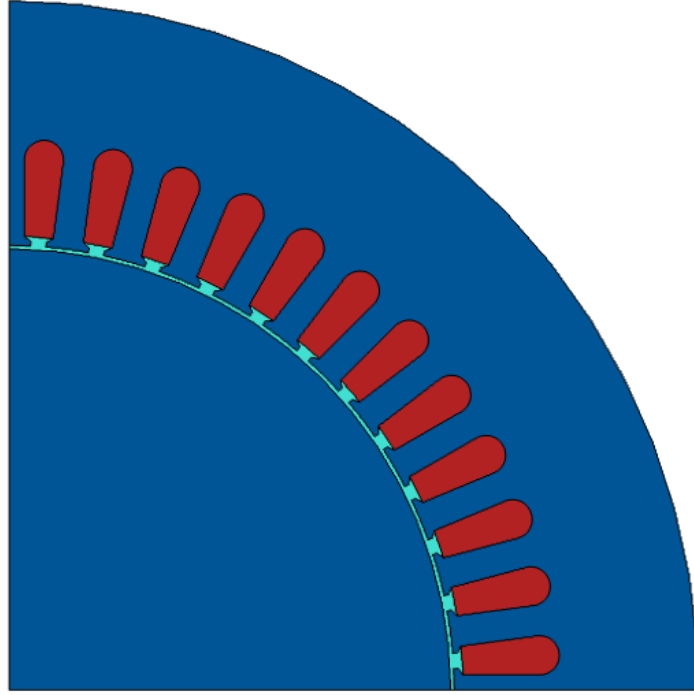
Figure 3.1: Model geometry in COMSOL

3.1.1 Material Properties

It is very important to define accurate material properties of the machine. COMSOL allows user to add the desired material from its library and customize it. Air is defined in gap between the stator and rotor and copper in the stator slots for modelling the winding. Relative permitivity and relative permeability of the copper is set to be 1 while electric conductivity equal to 6×10^7 S/m. The core of the stator and rotor is built from non-grain oriented laminated steel sheets $M400 - 50A$ [31]. Since modelling is to be done by taking into account the magnetic saturation of the iron as well, BH curve of the same material is used for more accurate estimation of the core losses by taking into account the non linear behaviour of the reluctivity curve as shown in Fig 3.2.

3.1.2 Methodology

In order to solve electromagnetic fields problem in the motor, $MagneticFields(mf)$ physics is added to the model. Since a quasi 3D geometry of the motor is formed, the effective length of the machine, which is 0.249m, is defined into the plane of geometry. Since there is no motion of rotor involved, following partial differential equations in their stationary form are being used to solve for magnetic fields in the
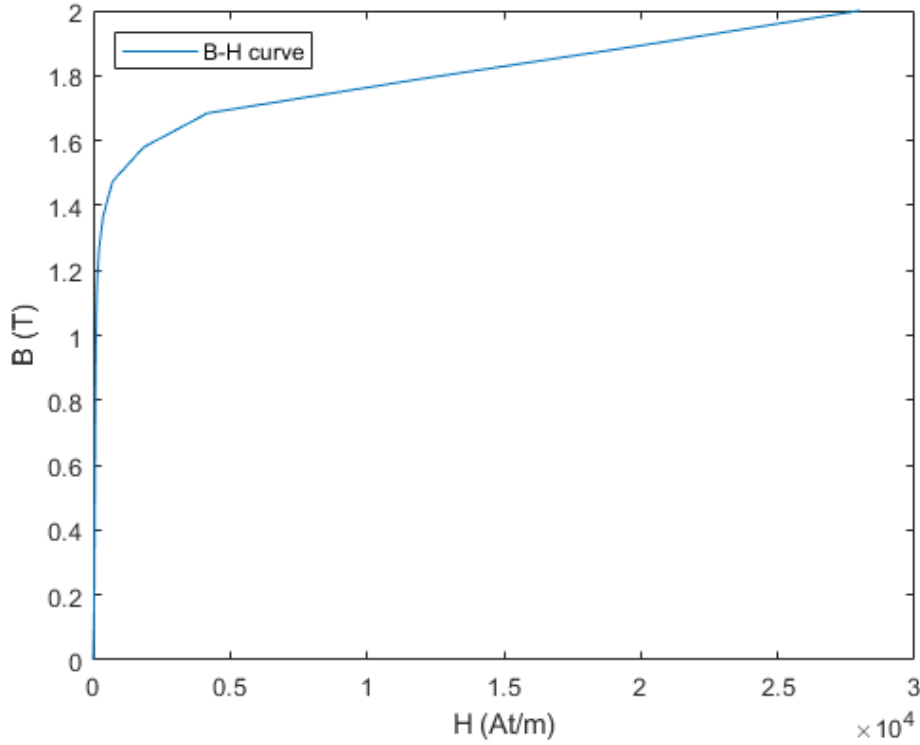
Figure 3.2: BH curve of iron core

problem domain

$$\boldsymbol{\nabla} \times \boldsymbol{H} \quad = \boldsymbol{J} \tag{3.8}$$

$$\boldsymbol{B} = \boldsymbol{\nabla} \times \boldsymbol{A} \tag{3.9}$$

Since we are using the symmetry of the motor assembly and modelling for only one pole of the machine, we need to define the appropriate boundary conditions as well. In Fig:3.3, anti-periodic boundary conditions has been applied on boundaries $B1$ and $B2$ according to which $A_{B1} = -A_{B2}$, where A is the magnetic vector potential. On the outer peripheral boundary of the stator, Dirichlet boundary conditions have been imposed i.e. $\boldsymbol{n} \times \boldsymbol{A} = 0$, which means there is a magnetic insulation on the outer boundary and all magnetic flux lines are conserved within that boundary. In order to model the winding, we define coils in magnetic fields physics and each coil corresponds to each phase of the 3 phase sinusoidal supply.

$$V_a = \hat{V} sin(\omega t) \tag{3.10}$$

$$V_b = \hat{V} sin(\omega t - 2\pi/3) \tag{3.11}$$

$$V_c = \hat{V} sin(\omega t - 4\pi/3) \tag{3.12}$$

Since there are 4 slots per pole per phase, the phase sequence of the distributed winding will be A+, C- and B+, where A,B and C correspond to each phase corresponding to its coil as shown in the Fig: 3.3. The negative sign of coil C shows the reverse direction of current with respect to coils A and B. Each coil is modelled as homogenized multi-turn coil in conductor model of coil settings.
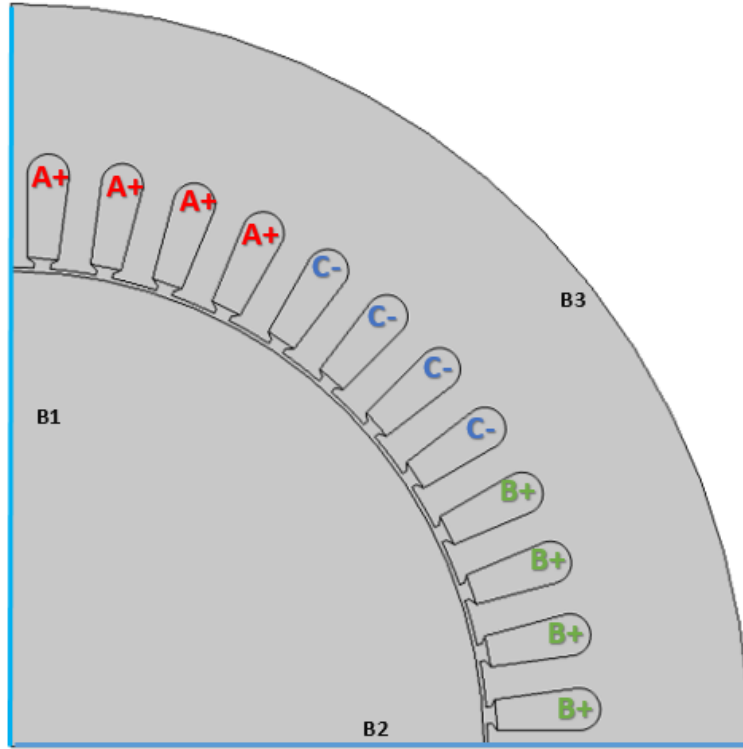
Figure 3.3: Winding sequence of coils in stator

In order to energise the coils, we can either feed it directly with 3 phase sinusoidal current source or with a voltage fed model by including external circuit physics to the model. A 3 phase, star connected, 50Hz voltage source, Eq.3.10 to Eq.3.12, is connected with the winding coils with external connecting resistance to build the rotating magnetic field in the motor as shown in Fig3.4 The corresponding stator phase equations are given below

$$V_{\text{a}} = I_{\text{a}} R_{\text{a}} + \frac{d\psi_{\text{a}}}{dt} \tag{3.13}$$

$$V_{\text{b}} = I_{\text{b}} R_{\text{b}} + \frac{d\psi_{\text{b}}}{dt} \tag{3.14}$$

$$V_{\text{c}} = I_{\text{c}} R_{\text{c}} + \frac{d\psi_{\text{c}}}{dt} \tag{3.15}$$
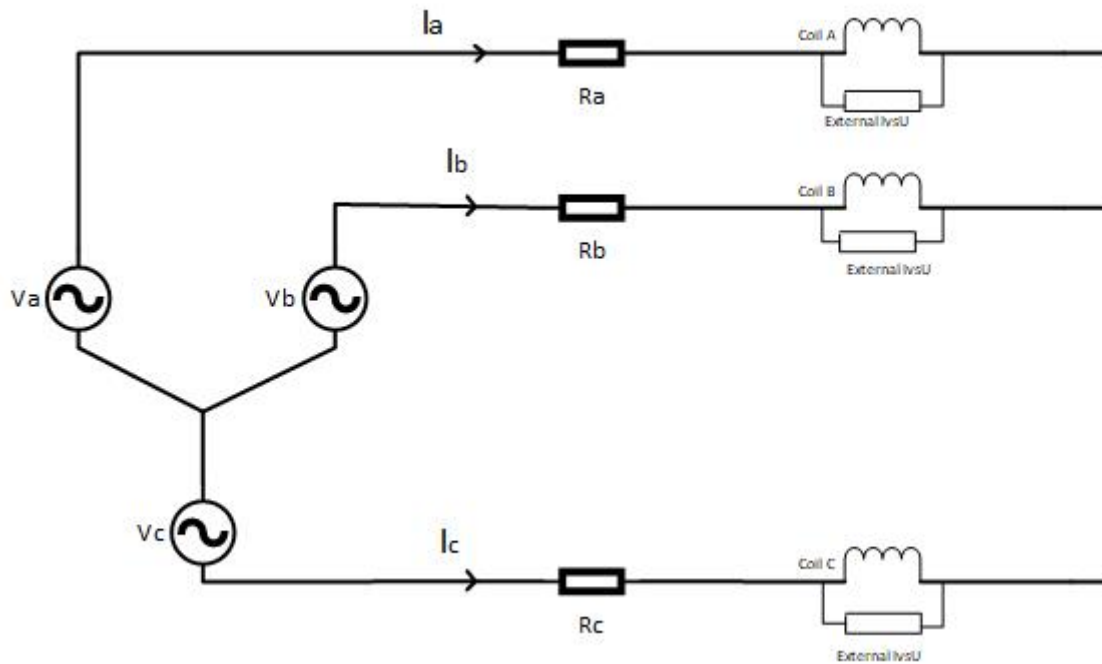
Figure 3.4: External Circuit

3.1.3   Mesh and Post-processing

The estimation of solution of any physical problem in finite element analysis depends upon the discretization of the problem domain into a number of discrete finite elements. For this purpose, a mesh of free triangular elements has been created in the problem domain. The density and quality of mesh are directly related to the accuracy of the converged result since it increases the degree of freedom of the solution but as the mesh is made finer, the problem becomes more computationally challenging and time taking. Fig.3.5 shows the resulting mesh being created for the built geometry.
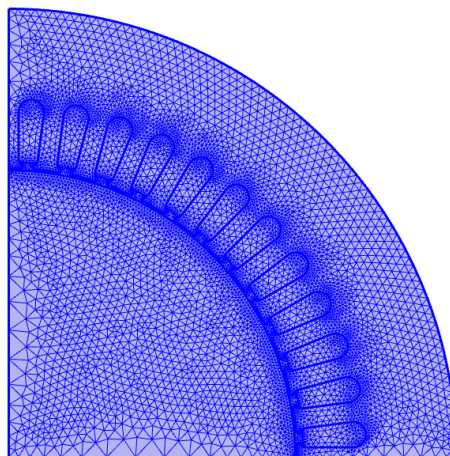
Figure 3.5: Mesh of the geometry

After setting up equations and mesh for the magnetic field analysis in the machine, the problem is solved by the stationary and time dependent solver. The stationary study step in COMSOL is used when field variables do not change over time. Stationary study is followed by the time dependent analysis of the problem in which transition of field variables are observed over a defined period of time. For accurate and efficient solution of the problem in the time domain, time stepping is done by Generalized Alpha method with maximum step size of 0.0001 seconds. Inbuilt solver, PARDISO, is used as solver with fully coupled settings using automatic Newton as linear solver. When stator windings are energized at rated voltage i.e. 400V, the resulting magnetic field distribution can be seen in Fig:3.6 The coil parameters such as applied voltage and resulting coil current variation in time is shown in Fig:3.7 and Fig:3.8 respectively. The voltage being applied is purely sinusoidal but coil current induced at rated voltage shows some transition in the first 2 cycles after which it get stabilized with some harmonic contents showing the saturation effect due to non linearity which will be computed during loss calculation in the next topic.
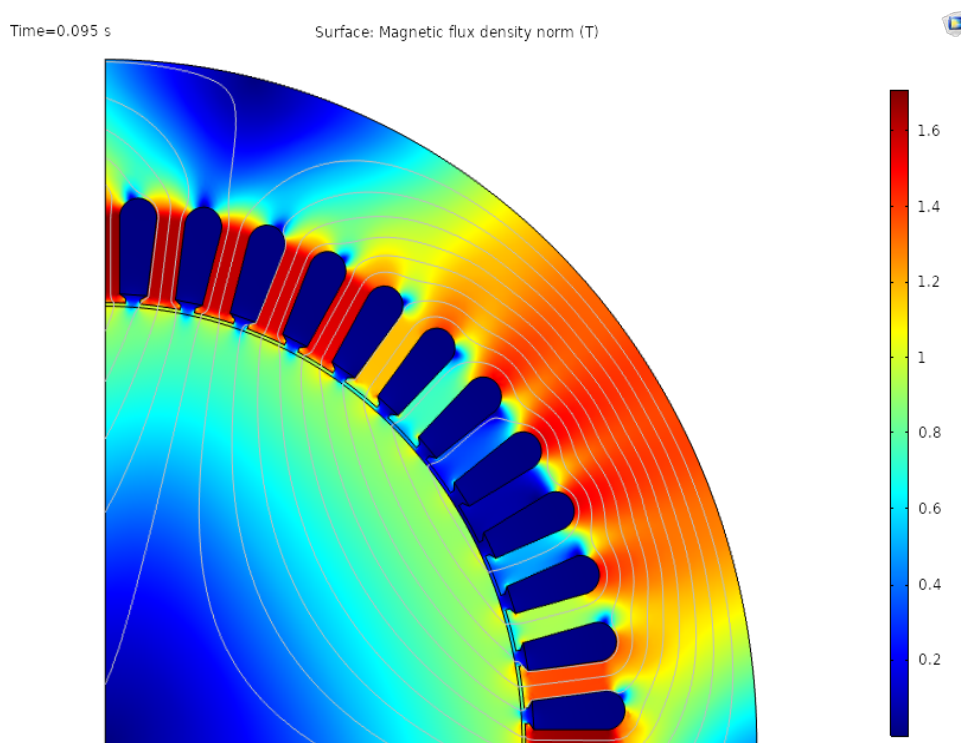
Figure 3.6: Magnetic Flux Density norm (T)
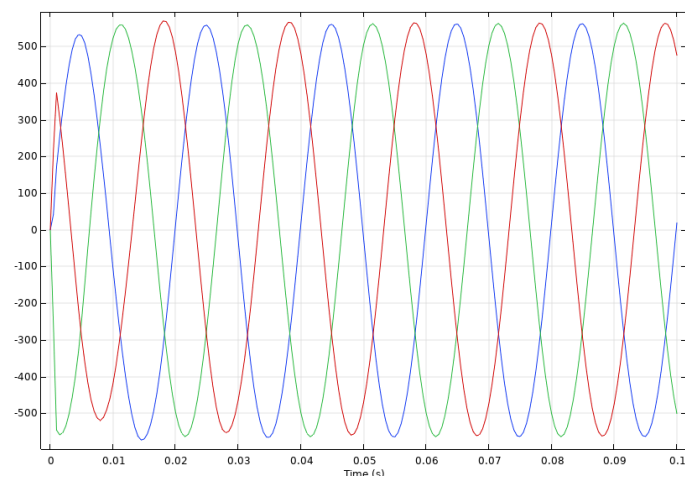
Figure 3.7: Stator Voltage
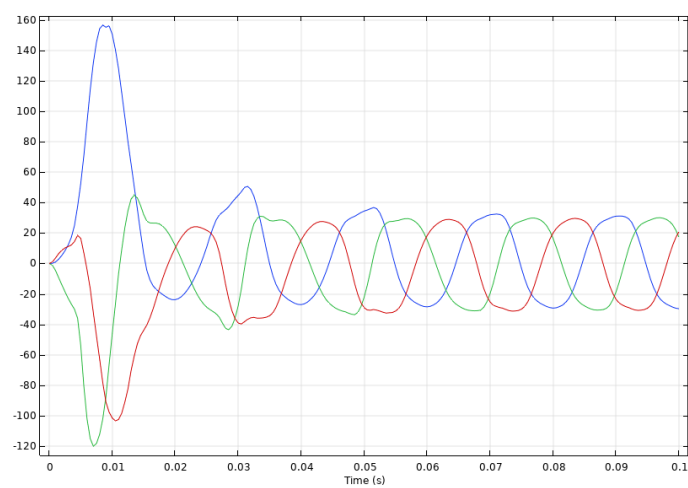
Figure 3.8: Coil Current

3.2   Iron Loss Computation

To identify the different loss components of the iron losses, the COMSOL model was integrated with the matlab software via livelink to matlab through which it is possible to access COMSOL model. The geometry of the problem domain is dicretised by creating a meshgrid of rotor and stator separately which basically divides the whole surface area of the stator and rotor in number of small elements. There are total of 60,000 elements of meshgrid created for rotor and stator separately and COMSOL model is run remotely from MATLAB to get magnetic flux density in each of the element of meshgrid individually. Fig.3.9 shows the x,y and normal component of the magnetic flux density in 10900th element over a period of one cycle.
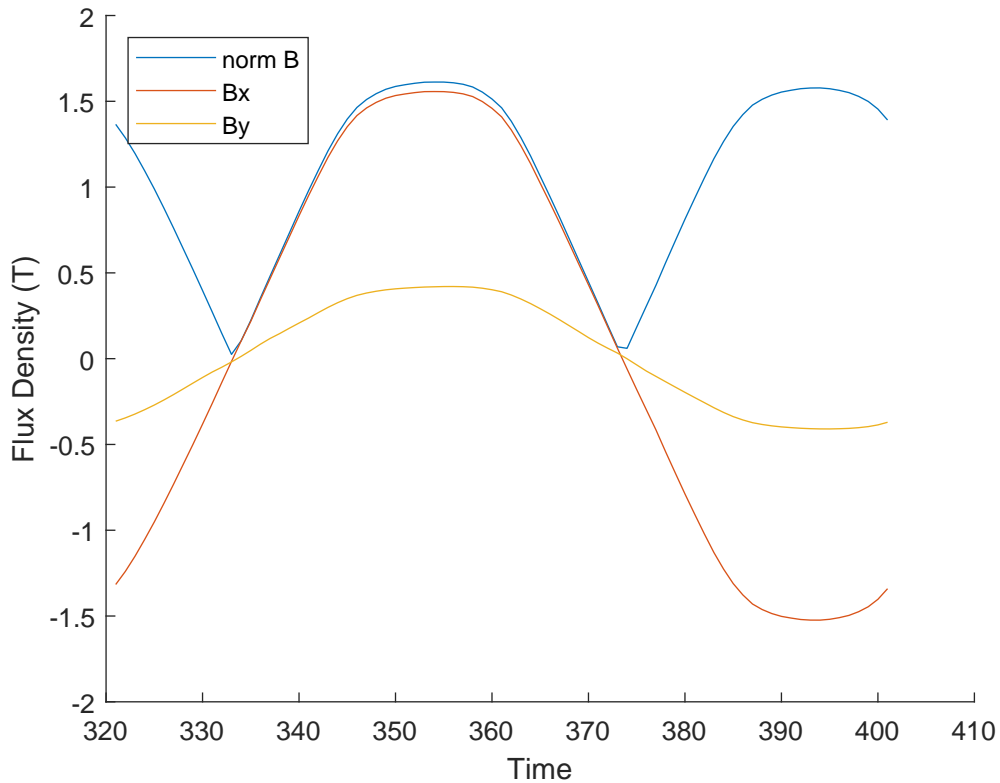
Figure 3.9: Magnetic Flux Density in meshgrid element

The distortion in the sinusoidal waveform of magnetic flux density implies the saturation effect of material occurring at rated voltage. So in order to compute losses from the magnetic field, taking the peak value of magnetic field will not give accurate results due to presence of harmonics. To find the weight of each harmonic component, fast fourier transform of magnetic field waveform in each element is done. Fig.3.10 shows the peak values of the harmonics of magnetic field waveform in the same element.
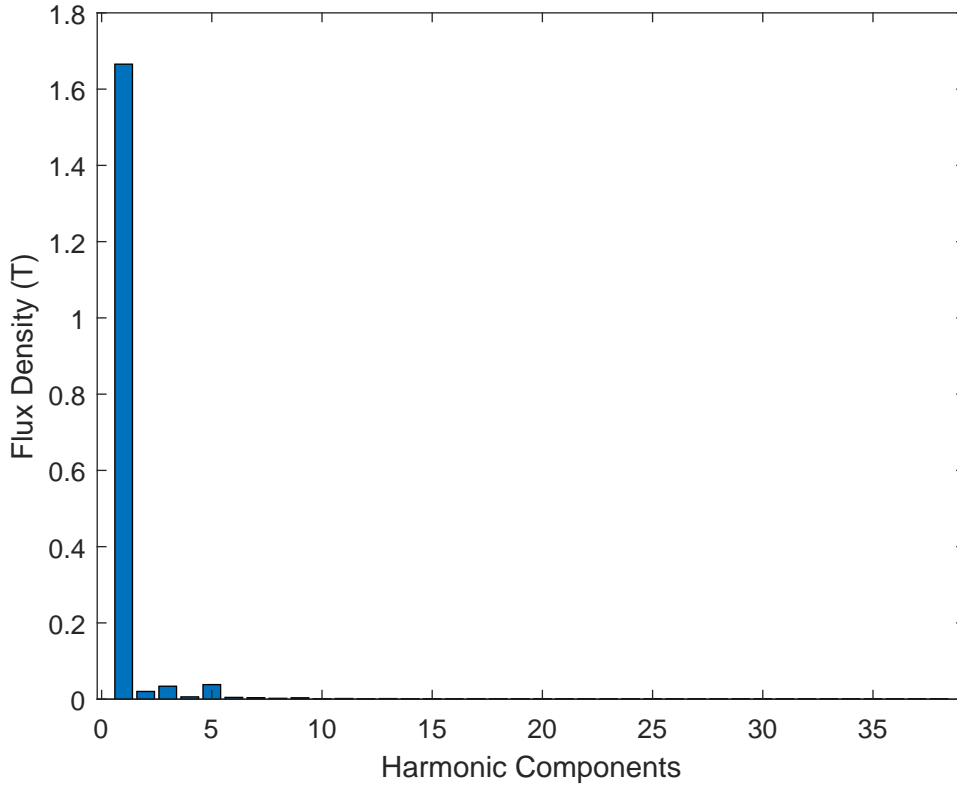
Figure 3.10: Fourier Transform of Magnetic Flux Density

Once we find the harmonic content of the flux density in each element of the meshgrid, the specific core loss in watts per kilogram can be computed from the following relation

$$W_{\text{Fe}} = K_{\text{h}}\, fB^{\alpha} + K_{\text{e}}\, f^2 B^2 + K_{\text{ex}}\, f^{1.5} B^{1.5} \tag{3.16}$$

where W_{Fe} is the total iron loss in W/kg, K_h, α, K_e and K_{ex} are the coefficients of hysteresis, eddy current and excess loss respectively. These coefficients are computed using the multi frequency Epstein tests [32].The total specific iron loss in W/kg is found by summation of loss occurring individual element due to all harmonic components of the magnetic fields. The density of the material is taken to be 7700 kg/m^3 and knowing the volume of the machine, total iron losses in watts is computed. These losses are further used for comparison with the measured losses and in the forward thermal model of the machine for temperature distribution study.

3.3 Thermal Modelling

After the computation of losses occurring in the stator, rotor and winding of the motor, the next step is to model the thermal behaviour of the machine. The temperature rise in the motor due to losses occurring in the different parts of the machine, needs to be evaluated and for this purpose, COMSOL Multiphysics has been used to predict the temperature profile in the machine using finite element analysis.

3.3.1 Geometry and Material Properties

The first step for thermal modelling in COMSOL is setting up motor geometry. For this purpose, a 3D model of the motor is built comprising of stator, rotor, air gap, winding, end winding, rotor shaft and end plates of the rotor as shown in the Fig. 3.11. Again instead of modelling the whole geometry of the machine, which would make the problem computationally challenging, the symmetry of the motor has been used and only $1/8^{th}$ of the complete geometry. Symmetric boundary conditions have been applied to the boundaries where there is continuity in the geometry.
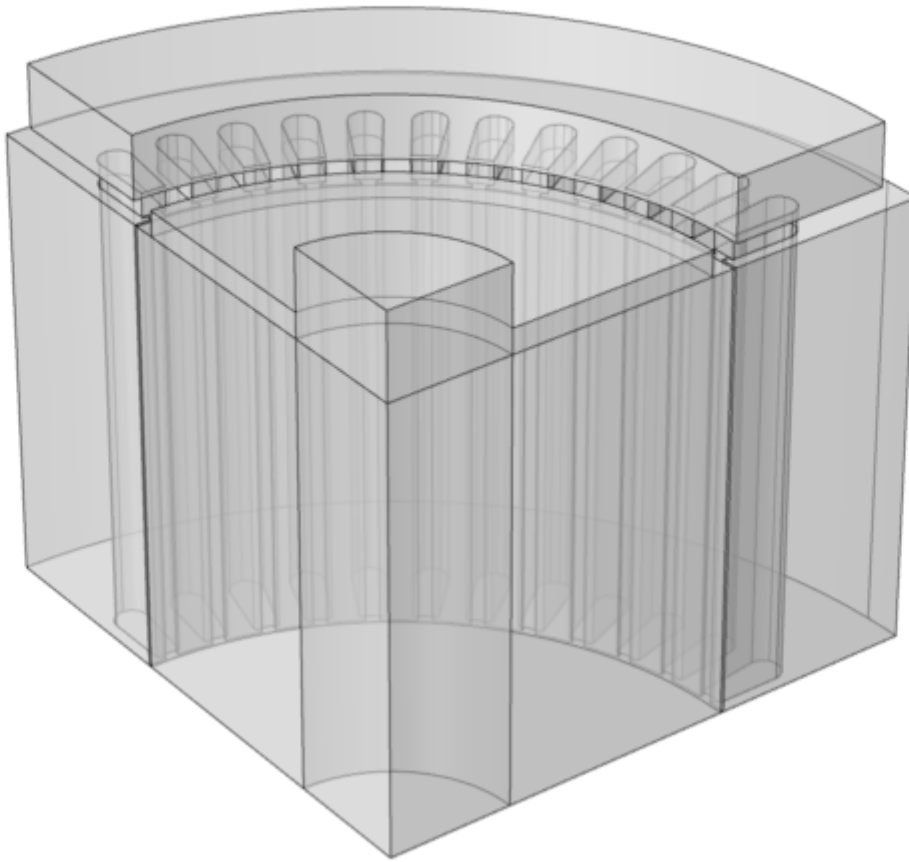
Figure 3.11: 3-D geometry of the motor

From the COMSOL material library, the relevant materials have been assigned to the respective domains in the geometry which includes, soft iron for the stator and rotor of the machine, copper for the winding and end winding, air for the air gap and structural steel for the shaft and end plates of the rotor. Material specific properties such as density, specific heat and thermal conductivity of the materials is assigned separately as shown in the Table 3.2.

The effective thermal conductivity, density and specific heat of the material is computed using Hashin and Shtrikman approximation [33] [34] as following. For example in the copper winding inside the stator slot, the thermal conductivity is

Table 3.2: Material properties in thermal model

Material	Thermal Conductivity $k_h[W/mK]$	Specific Heat Capacity $C_p[J/kgK]$	Density $\rho[kg/m^3]$
Copper	385	392	8890
Electric steel sheet	22-40 (lamination direction) 0.6(normal to lamination)	490	7700
Epoxy Resin	0.4	600	1540
Structural Steel	44.5	475	7850

maximum in the lapping direction and minimum in the perpendicular direction i.e.

$$K_{\text{hwp}} = f_{\text{wi}} K_{\text{h\_co}} + (1 - f_{\text{wi}})K_{\text{he}} \tag{3.17}$$

$$K_{\text{hw}} = K_{\text{he}} \frac{(1 + f_{\text{wi}})K_{\text{hco}} + (1 + (1 - f_{\text{wi}}))K_{\text{he}}}{(1 - f_{\text{wi}})K_{\text{hco}} + (1 + (1 - f_{\text{wi}}))K_{\text{he}}} \tag{3.18}$$

where K_{hwp} and K_{hw} are the thermal conductivity of the winding in the lapping and perpendicular directions respectively, K_{he} is the thermal conductivity of the epoxy, f_{wi} is the winding filling factor of copper, K_{hco} is the copper thermal conductivity. The effective density and specific heat capacity can also be estimates as following

$$C_{\text{pwi}} = f_{\text{wi}} C_{\text{pco}} + (1 - f_{\text{wi}})C_{\text{pe}} \tag{3.19}$$

$$\rho_{\text{wi}} = f_{\text{wi}} \rho_{\text{co}} + (1 - f_{\text{wi}})\rho_{\text{e}} \tag{3.20}$$

where ρ_{co} and C_{pco} are the density and specific heat capacity of the copper and ρ_{e}, C_{pe} are the respective density and specific heat capacity of the epoxy resin used in impregnating the winding. The winding filling factor f_{wi} is taken to be 0.65. The same criteria can be applied to the lamination of stator and rotor in which the maximum thermal conductivity is in the direction of lamination and its minimum in the direction perpendicular to the lamination due to presence of insulation layers between the sheets. The stacking factor for the stator and rotor sheets is taken to be 0.95.

3.3.2 Heat Transfer Physics

Once geometry and material properties for different domains of the motor model have been defined, we need to add the the relevant physics to our model which are governed by set of differential equation to compute the resulting temperature distribution in the motor. In order to achieve this, heat transfer in solids interface from COMSOL physics library is added which is particularly useful to model heat transfer in solids by conduction, convection and radiation. The temperature equations which are defined in solid domains incorporate the differential form of Fourier's law which take into account different heat sources as well. As mentioned earlier that we are modelling

only $1/8^{th}$ of the total geometry of the motor, the respective symmetric boundary condition are also defined in this interface.

Since the motor has blocked rotor, so only sources of heat are iron losses occurring in the stator and rotor along-with copper losses in the winding of the machine. The iron loss computed in the stator and rotor in the previous section are input into the domains of stator and rotor separately where as copper losses are split into two different sources due to complexity of their geometry. Part of winding which is inside the stator core is defined as separate source of heat whereas end windings are defined as a separate heat source as following

$$P_{\text{cu,s}} = 3\left(\frac{I_{\text{rms}}}{2}\right)^2 R_{\text{cu,s}} \tag{3.21}$$

$$P_{\text{cu,ew}} = 3\left(\frac{I_{\text{rms}}}{2}\right)^2 R_{\text{cu,ew}} \tag{3.22}$$

where $P_{\text{cu,s}}$ and $P_{\text{cu,ew}}$ are the heat source in the copper winding in the stator slots and end winding respectively while $R_{\text{cu,s}}$ and $R_{\text{cu,ew}}$ are the resistances of the copper in the stator slots and end winding. Since the resistance increases with the rise in temperature, the copper losses are put as a function of temperature to take this change of power into account. The total resistive power loss as a fuction of temperature rise can be calculated using Eq.3.23.

$$P_{\text{cu}} = P_{\text{w}}\left(1 + \alpha(T - T_{\text{amb}})\right) \tag{3.23}$$

where α is the temperature resistance coefficient and is equal to 0.004041 for copper, T_{amb} is the ambient temperature and T is the winding temperature. Once all the heat sources have been defined, next we need to define boundaries where heat flux will take place which is mostly the external surfaces of the stator, rotor and end winding exposed to external environment. As the temperature of the motor increases, a negative heat flux will take place depending upon the convective coefficient as following

$$q_{\text{o}} = h\left(T_{\text{ext}} - T\right) \tag{3.24}$$

where h is the convective coefficient $[W/m^2.K]$. These heat flux boundaries are being applied on the external surface of stator, end winding and rotor surface towards end winding. After setting up all the physics parameters, next we need to create the mesh of the geometry in order to solve the set of partial differential equations governing the heat transfer mechanism via finite element analysis. A mesh is being created with combination of tetrahedrons, triangles, edge and vertex elements in the mesh node of the COMSOL Multiphysics as shown in the Fig 3.12.

A time stepping analysis of the problem is done using the time dependent iterative linear solver of GMRES (Generalized Minimum RESidual) available with minimum residual tolerance of 0.01, in the COMSOL Multiphysics study nodes. The heat profile generated in the motor for different input values of the losses and currents will be shown in the following chapter in comparison to the measured temperature tests.
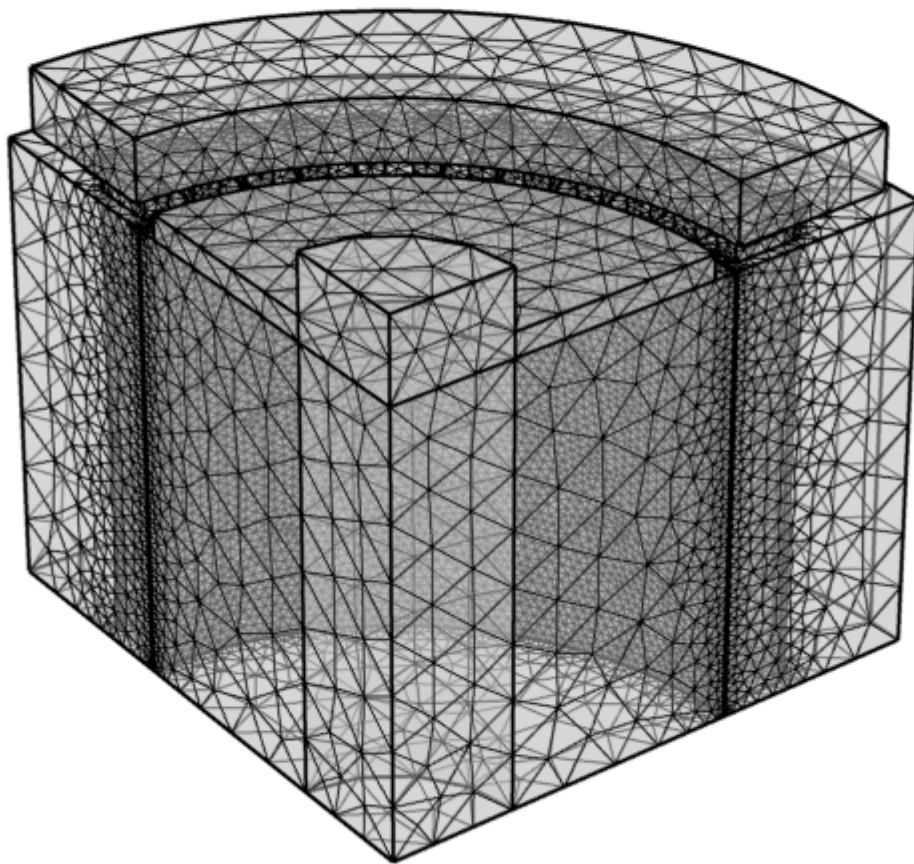
Figure 3.12: 3-D mesh of the motor geometry

4 Experiments and Results

In order to verify the electromagnetic and thermal models of the induction motor, it was subjected to different measurements under different voltages and flux densities to get the losses and temperature distribution measurements in the laboratory, details of which is explain the following section.

4.1 Experimental Setup

The motor on which electromagnetic and thermal modelling is done in the previous chapters was 37kW cage induction motor and same actual motor with identical set of design parameters was needed for measurements to validate the results. The stator of the machine was built from M400 50a laminated sheets of 0.5[mm] thickness with laser cutting and stacked together as per design. From experiments, the targets measurement data for comparison and analysis was as following

- Line Voltage.

- Current.

- Winding Resistance.

- Total Input power.

- Temperature rise data in stator end winding.

The stator of the machine was energized with a supply from a synchronous generator instead of supply from grid in order to get variable voltage supply, constant frequency and pure sinusoidal voltage to make it as close to one considered in simulation models. For the measurement of the temperature at different points in the machine, PT100 sensors with 4 wire termination were used. These sensors give highly accurate temperature measurement results in the range of -50°C to 250°C. Their reference resistance is 100Ω at 0°C with accuracy of +/- 0.06°C. The target area for the measurements of temperature were inside the stator core and end winding. 3 PT1000 sensors were embedded in each phase of the end winding of the stator but for the temperature measurement inside the core, these sensors were soldered on a 6[mm] thick PCB sheet designed to perfectly match the geometry of the stator as shown in the Fig. 4.1

There are 6 PT100 sensors soldered in the region of each pole of the stator including the teeth of core. In the manufacturing of the stator, the laminated sheets are stacked, compressed with about 60 Tons of force before welding at 13 along the outer periphery of the stator. So, in order to save the sensors from destroying by the compression force, 13 reinforced shims made of same iron sheets were cut with thickness of 1[mm], greater than thickness of the PCB sheet, were placed in line with the welding points to absorb the compression force. Additionally, thermally conducting but electrically insulating tape was used to cover the sensors as shown in the Fig. 4.2 where end connection projections are coming outside of the stator for end connections with the temperature measurement setup.
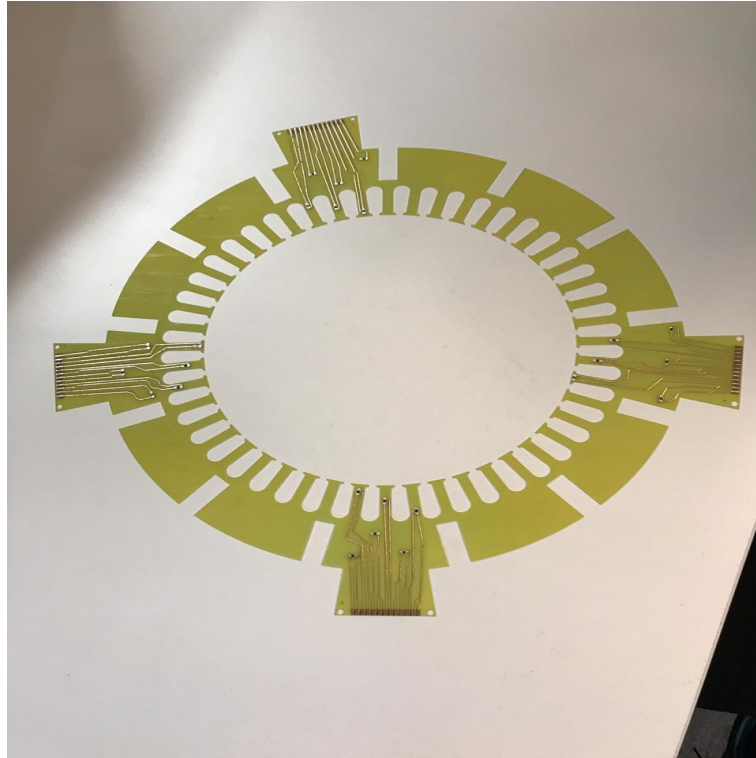
Figure 4.1: PCB sheet of sensors

4.2 Simulation and Measurement Results

The electromagnetic model is used to compute the iron loss occurring in the stator and rotor of the machine at different voltages and flux densities. A three phase sinusodal voltage source in electric circuit physics of the COMSOL Multiphysics is coupled with the coils of the induction motor and resulting iron loss occuring in the stator and rotor are listed in the Table 4.1

Table 4.1: Simulated Iron loss of machine

Voltage V	Current I	Frequency Hz	Stator Iron loss W	Rotor Iron loss W	Total Iron loss W
50	2.76	50	6.11	2.05	8.17
100	5.53	50	21.84	7.31	29.15
200	10.94	50	69.78	24.36	94.14
300	16.4	50	138.1	46.88	184.98
400	23.6	50	264.83	76.87	341.7

In order to validate the simulated iron loss results, the induction machine was energized with the same voltage levels from a synchronous generator at 50 Hz frequency. The input power calculated from the measurement setup gives total power being fed to the motor, consumed in the stator, rotor and the copper losses. Before the measurement, the resistance of the stator winding was measured which was
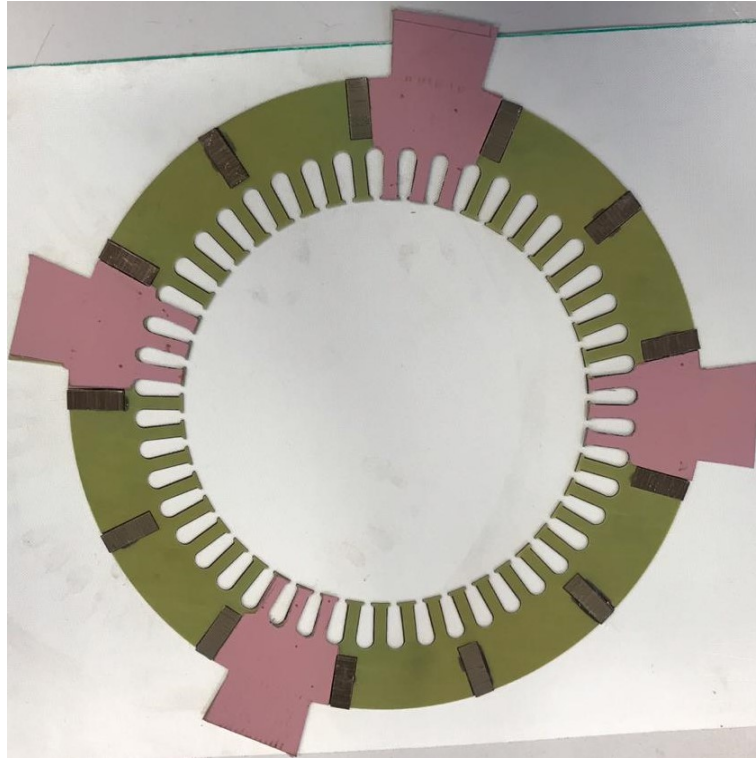
Figure 4.2: PCB sheet of sensors with shims

0.075Ω per phase. Knowing the line current and the resistance of winding, the copper losses can easily be computed and rest of the input power corresponds to iron losses of stator and rotor.

Table 4.2: Measured Iron loss of the machine

Voltage	Current	Frequency	Copper Loss	Total Iron loss
V	I	Hz	W	W
50	2.76	50	6.11	11.03
100	5.53	50	21.84	37.4
200	11.25	50	28.48	113.52
300	17.1	50	65.79	214.38
400	25.3	50	144.02	363.15

The comparison of total measured and simulated loss shows that the simulated losses are lagging behind the corresponding measured iron loss as shown in the Fig 4.3. This difference can be explained due to the fact that iron sheets were cut by laser cutting technique which were not taken into account in the electromagnetic model and some excess losses. However, simulated loss gives a good insight to the loss division between the stator and rotor, where stator iron loss contribute the most to the total iron loss.

These stator and rotor iron losses were fed in the COMSOL Multiphysics thermal model as heat sources along with copper losses in the winding. In order to get
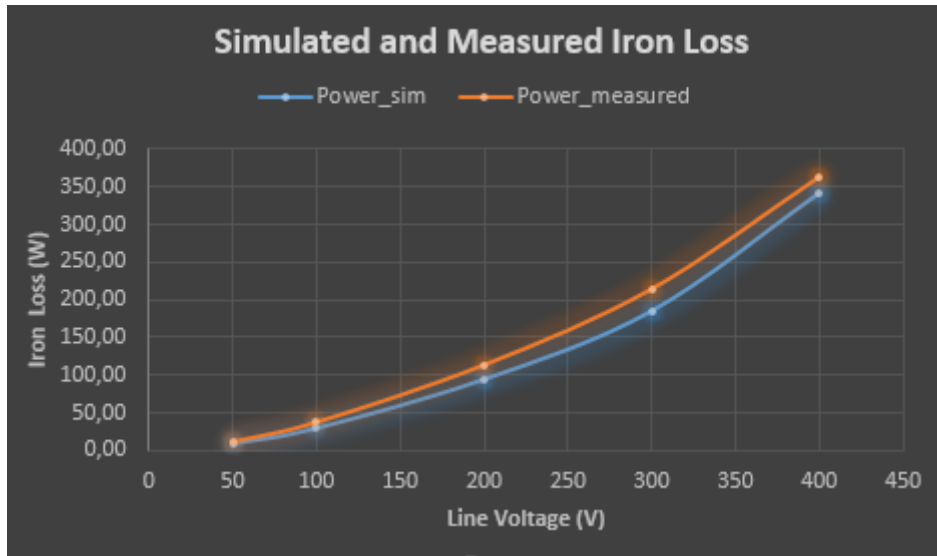
Figure 4.3: Simulated vs Measured Iron loss

the more accurate response of the thermal model, these losses were modified by scaling them to the measured values so that the temperature profile of the machine model can be compared with the measured temperature. This is done because by putting the simulated loss in the model will always give the lesser temperature than measured one because of difference of power from measured. The machine in the experiment was energized at 200V, 300V and 400V at 50Hz frequency to measure the temperature rise in the core and end winding. Since there were multiple sensors placed at different locations in the core and end winding, the temperature rise curves of these sensors show overlapping implying the temperature is almost uniformly distributed with maximum difference of less than half degree Celsius among different sensors as shown in the Fig 4.4-4.5. For the purpose of clarity, temperature data of only one of the sensors is compared with the point evaluation of the corresponding temperature rise in the thermal model.
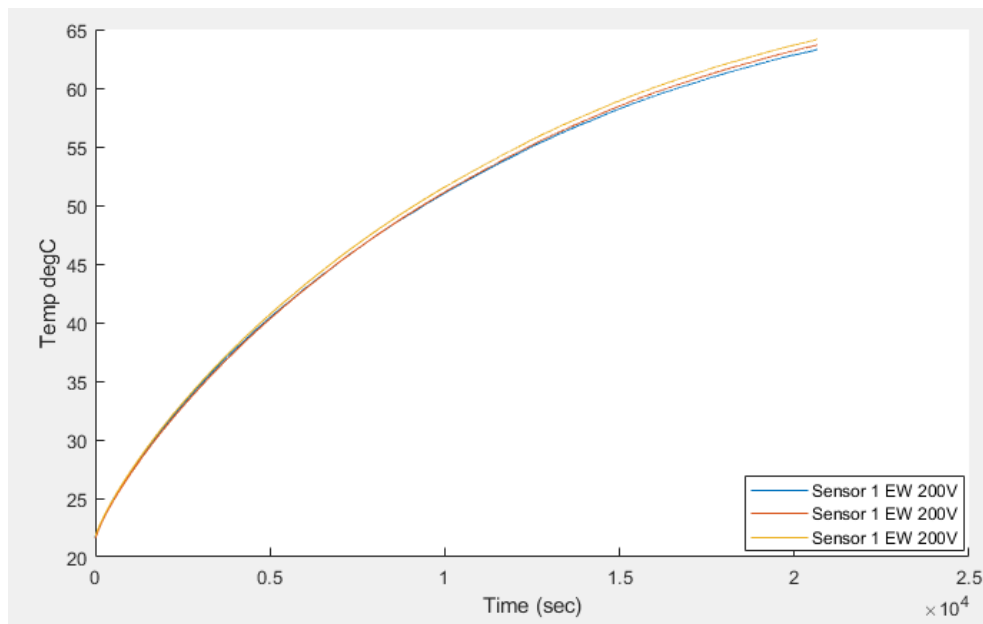
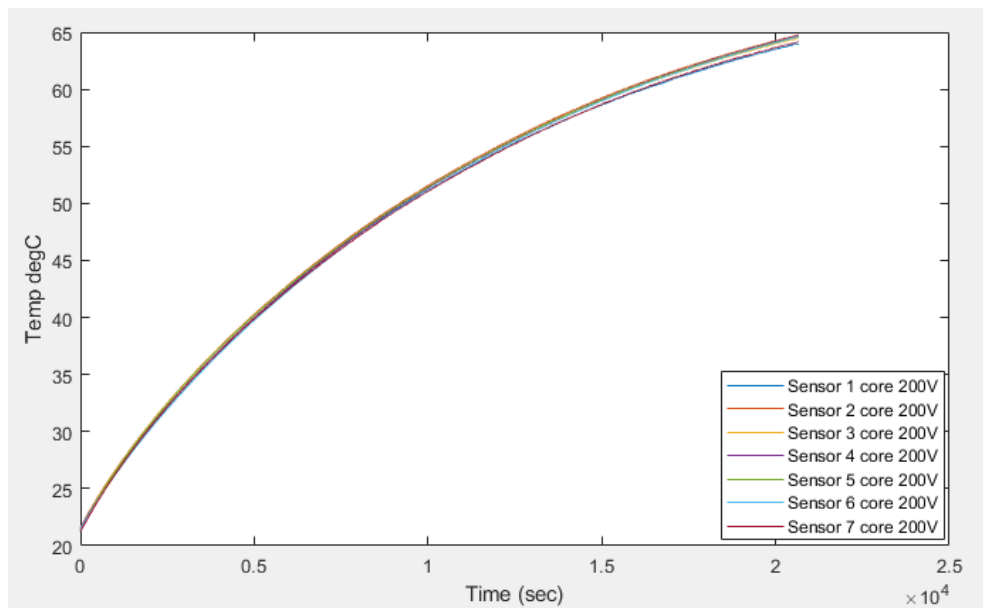Figure 4.4: End Winding measured temperature at 200V

Figure 4.5: Stator measured temperature at 200V

From Fig. 4.6-4.11 , the temperature rise comparison of the end winding and stator core is shown for the 200V, 300V and 400V respectively. These curves correspond to the initial temperature rise for 6 hours for the 200V and 300V while 3 hours for 400V measurement and simulated time. The natural convection coefficient for the model is within the range of 9-12$[W/m^2.K]$ corresponding to different boundaries in the geometry interfacing with the external atmosphere. The curves show a close similarity between the predicted temperature rise from COMSOL Multiphysics thermal model and actual temperature rise for the corresponding voltage conditions.
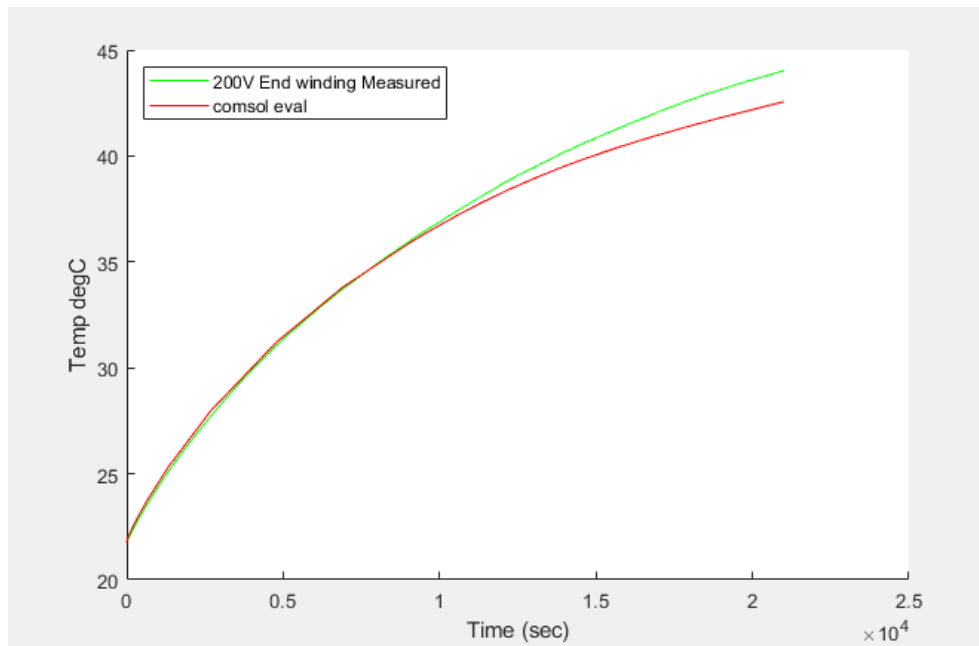
Figure 4.6: End Winding measured vs simulated temperature at 200V
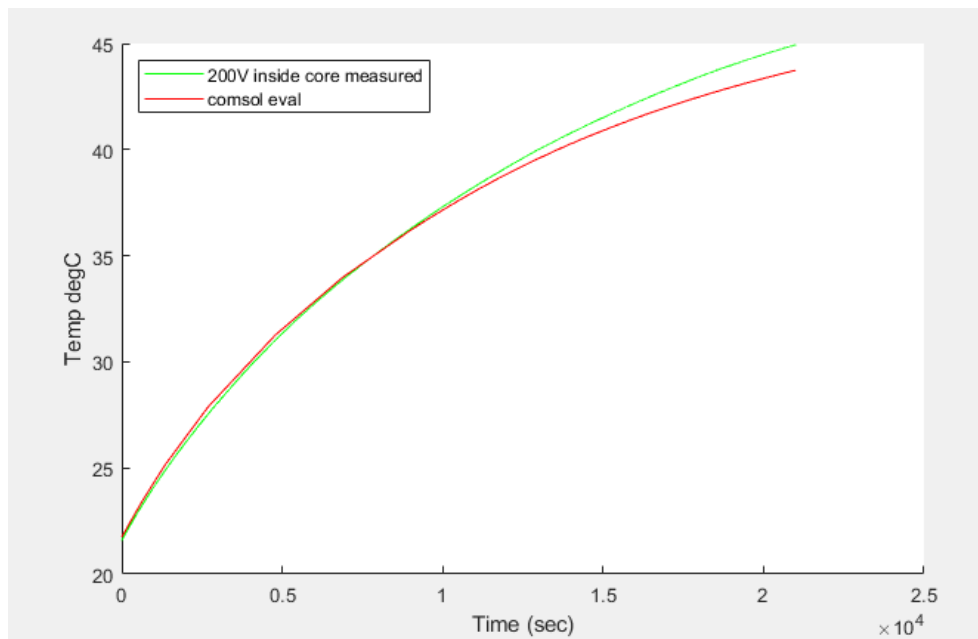
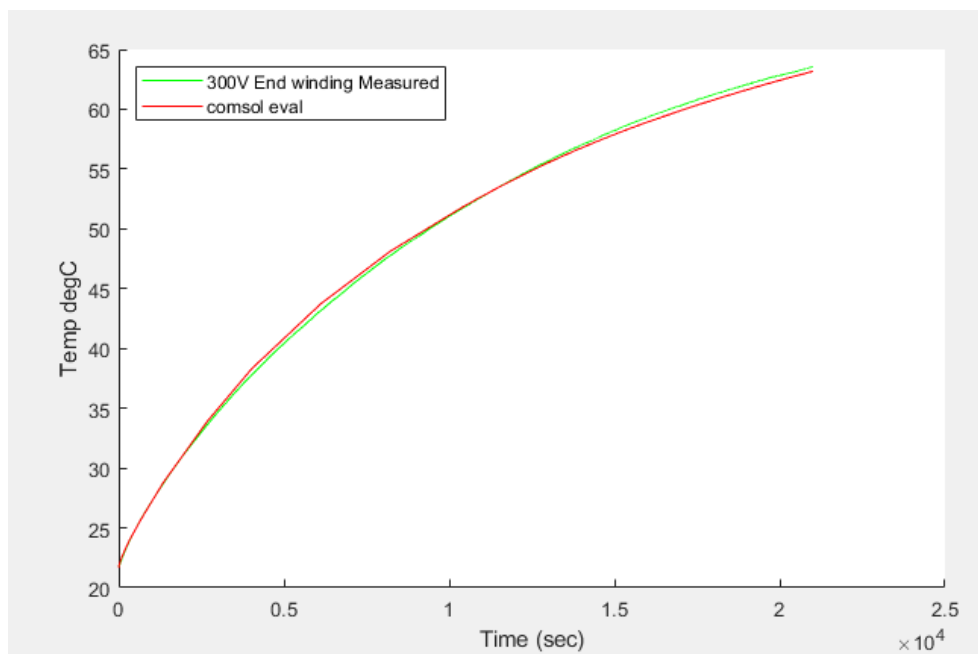Figure 4.7: Stator measured vs simulated temperature at 200V

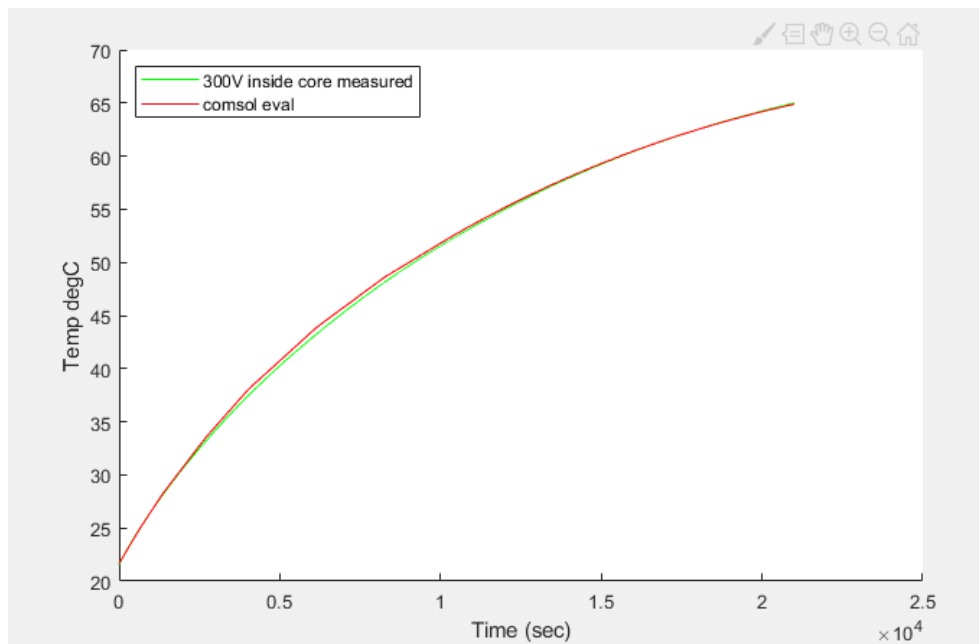Figure 4.8: End Winding measured vs simulated temperature at 300V

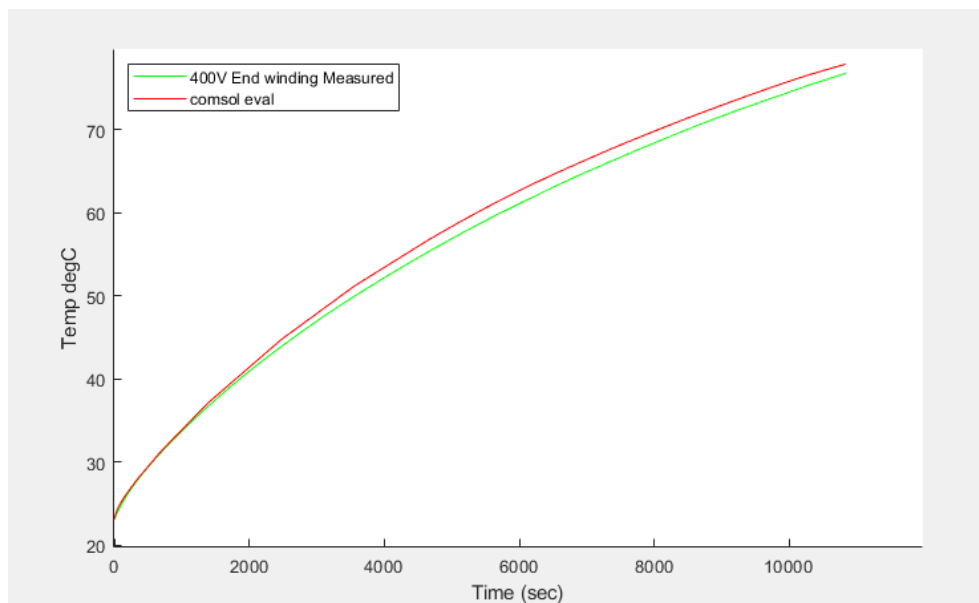Figure 4.9: Stator measured vs simulated temperature at 300V

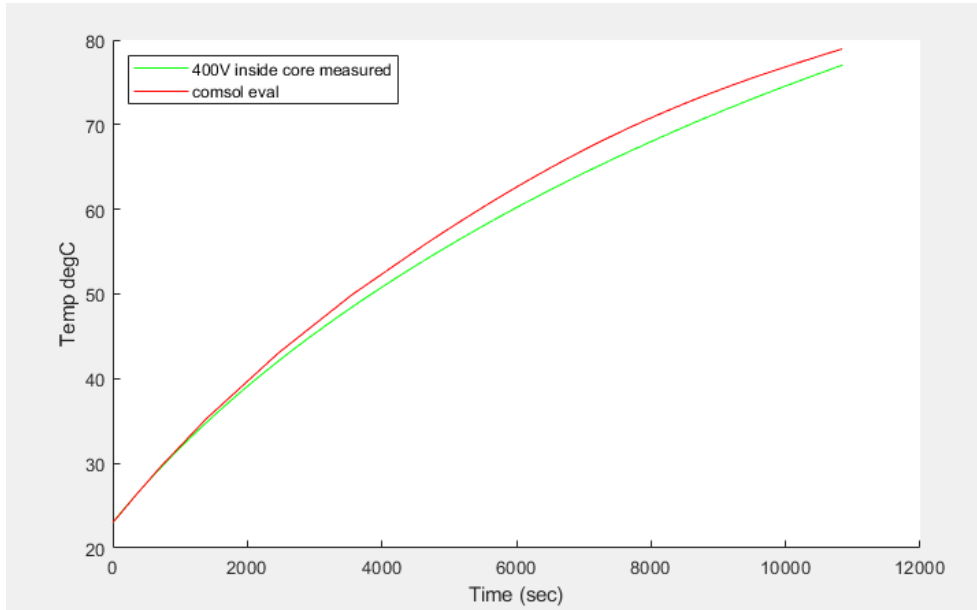Figure 4.10: End Winding measured vs simulated temperature at 400V

Figure 4.11: Stator measured vs simulated temperature at 400V

Since the test being performed under locked rotor condition, the time constant for the machine to reach steady state condition is quite big. However, to validate the steady state response of the model, the motor was energized at 300V for more that 12 hours to reach the steady state. The temperature rise measured for steady state conditions was compared with the temperature rise of the thermal model as shown in Fig 4.12-4.13 which shows quite accurate prediction of temperature rise in the stator core and end winding of the machine. Once machine reached the steady state, the power supply to the stator was cut off and the resistance of the winding was measured for cooling down curve. The average temperature of the winding was computed from the following relation for copper

$$R_{\mathrm{T}} = R_{\mathrm{o}} \left(\frac{T + 235^{o}C}{T_{\mathrm{o}} + 235^{o}C} \right) \tag{4.1}$$

where R_{T} is the resistance of the winding at temperature T, R_{o} is the resistance of the winding at room temperature T_{o} which was 0.075Ω at $224^{o}C$. The resistance R_{T} at the power cut off point was 0.09Ω. From 4.1, the average winding temperature at steady state came out to be $73.4^{o}C$. In the thermal model, the the volume average temperature for the complete winding domains at the steady state is $72.8^{o}C$. Fig4.14 shows the temperature distribution in the 3D thermal model of COMSOL in the steady state.
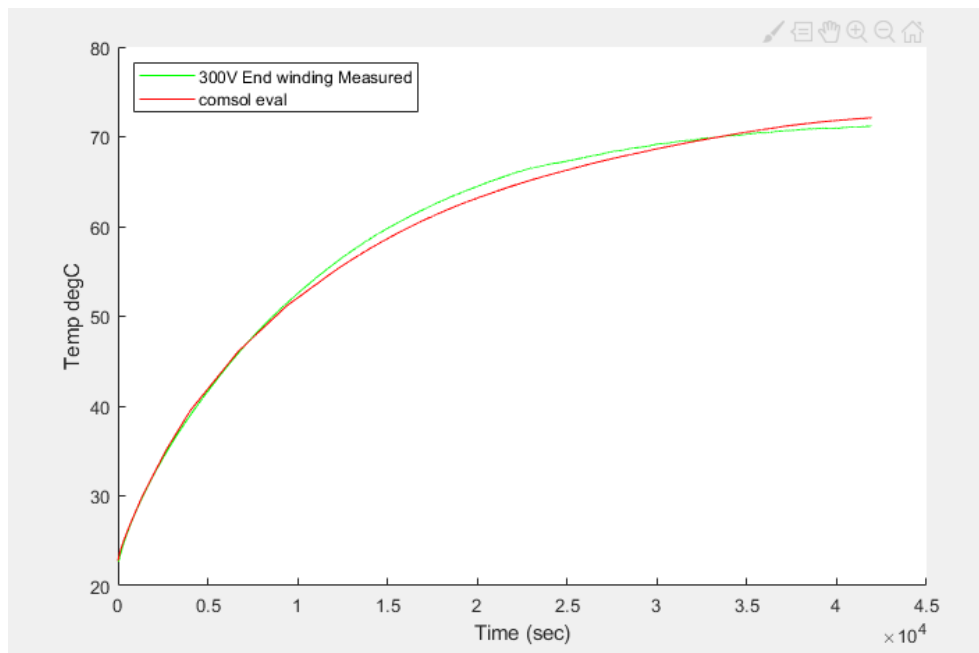
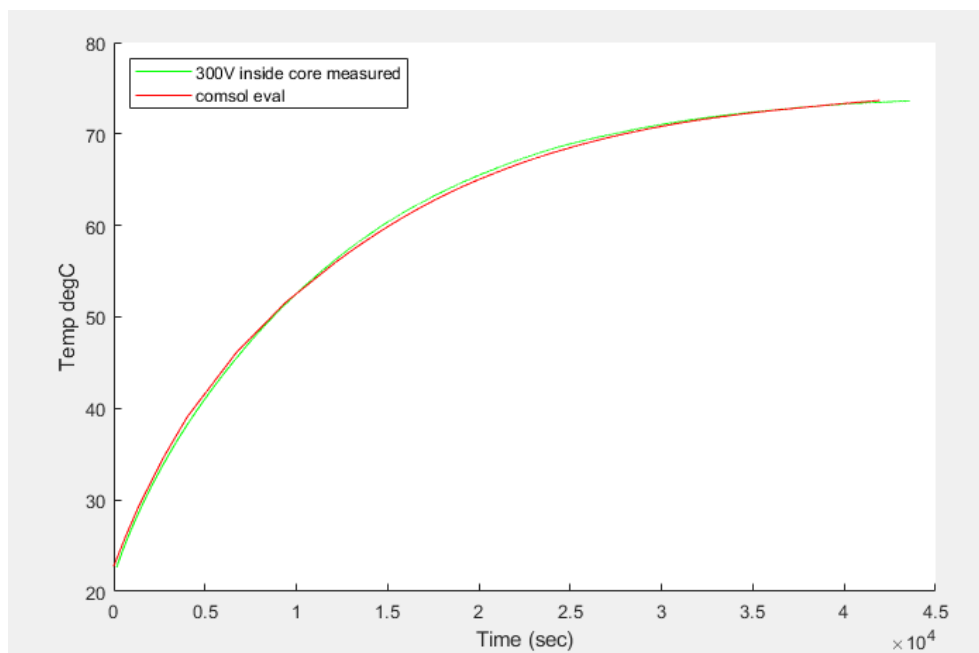Figure 4.12: Steady state End Winding measured vs simulated temperature at 300V

Figure 4.13: Steady state Stator measured vs simulated temperature at 300V

4.3 Inverse Thermal Modelling

The heat generated in the machine is basically due to losses occurring in the core or winding. Due to these losses, temperature of the machine rises and that temperature rise is proportional to the input heat. So on the basis of this principle, it is possible to estimate the loss in the machine from the rate of rise of temperature. When the
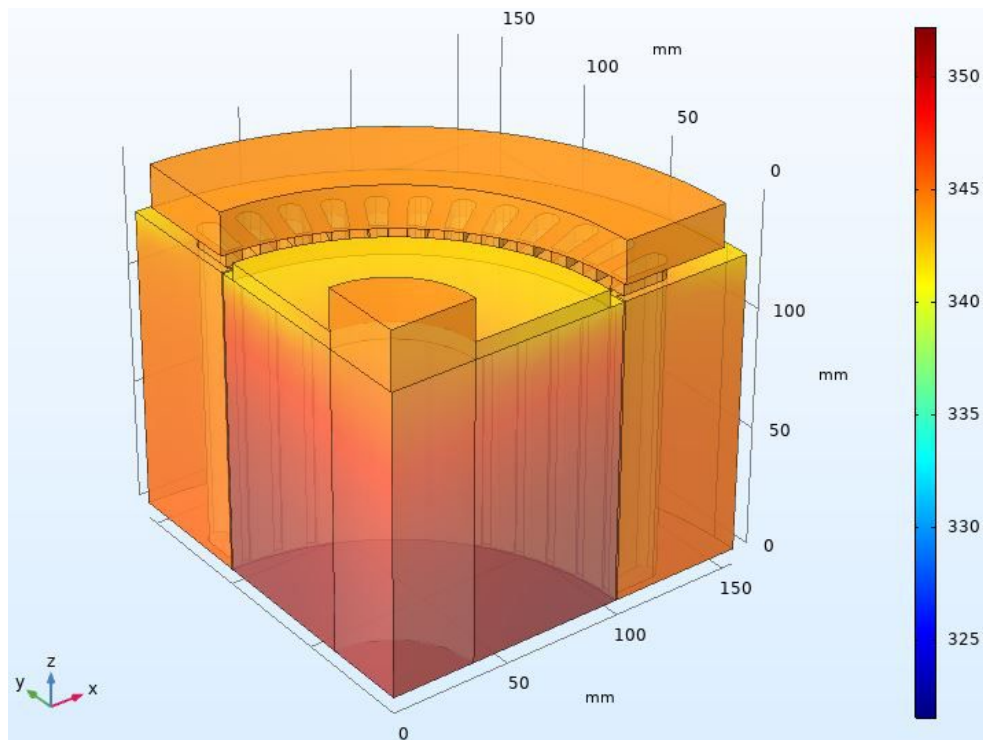
Figure 4.14: Steady state temperature distribution in COMSOL thermal model

machine is just energized, there is no effect of convection and all the heat being dissipated is owing to the conduction. The heat input and rate of rise of temperature can be related as following

$$q_c = \rho C \frac{\partial T}{\partial t} \tag{4.2}$$

This initial rate of rise of temperature was analysed for both measured and simulated temperature rise curves and the average slope of temperature times specific heat capacity and density of the iron give the loss occurring in the machine. Fig:4.15-4.17 shows a comparison of temperature rise in the core of the machine from the simulation and measurement.
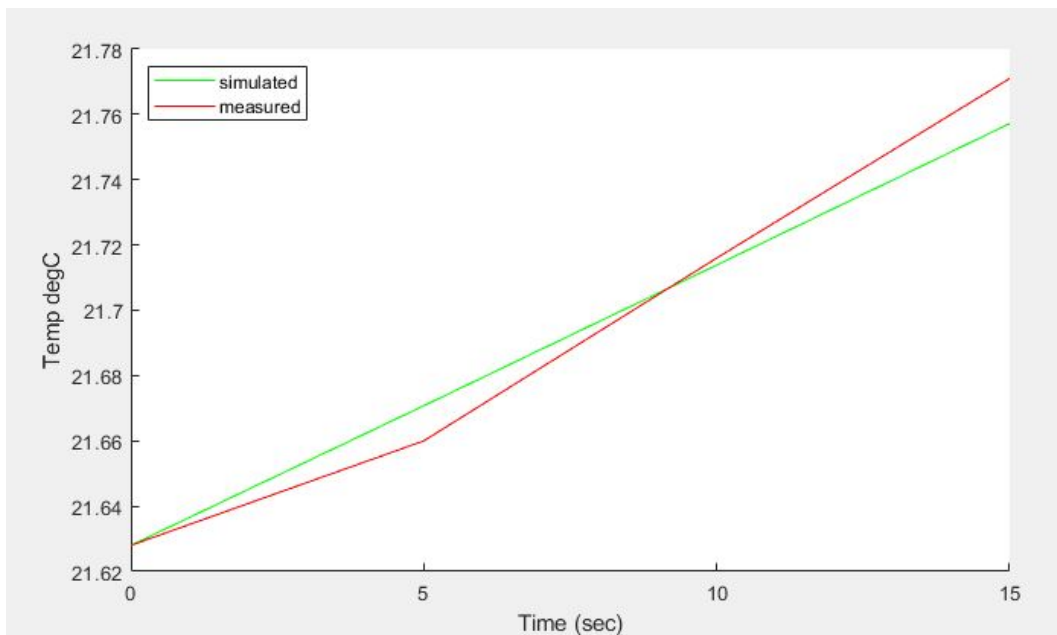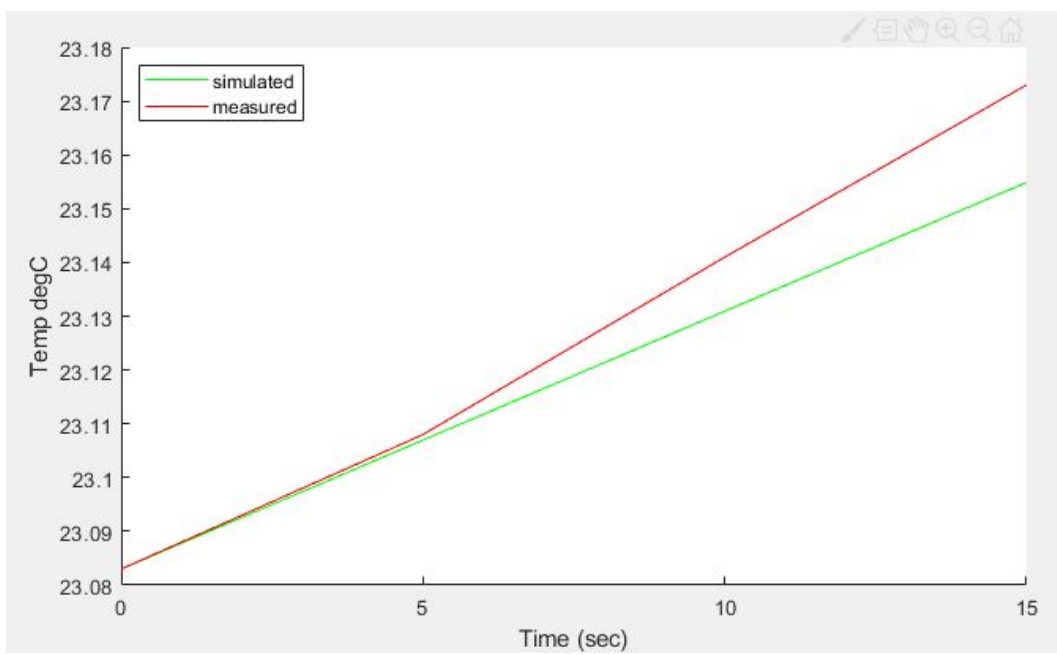
Figure 4.15: Initial temperature rise at 400V

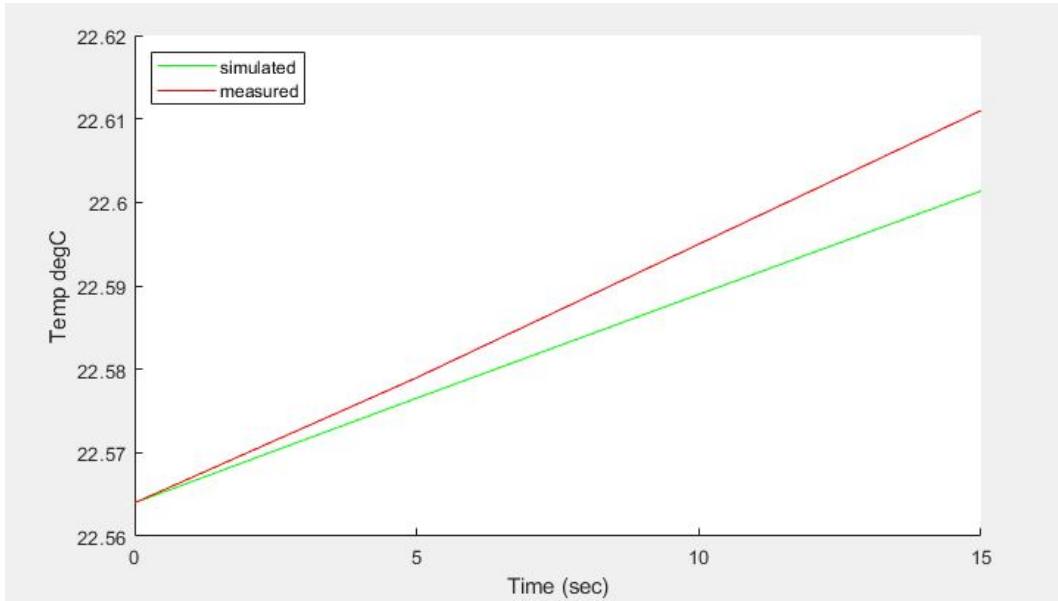Figure 4.16: Initial temperature rise at 300V

Figure 4.17: Initial temperature rise at 200V

It is evident from the figures that the slope of measured temperature is slightly bigger than the slope of initial temperature rise of the simulated model. In Table 4.3, a comparison of loss input to the stator of the thermal model is done with the inverse computation of the loss from the initial rate of rise of temperature in the stator core due to input loss. The error between these two losses shows that model temperature rise gives accurate inverse computation of the loss.

Table 4.3: Loss input to COMSOL model vs loss from simulated temp. slope

Voltage	Stator Iron loss	Loss from simulated temp.	Error
$400V$	$281W$	$272W$	3%
$300V$	$160W$	$159W$	0.6%
$200V$	$85W$	$83W$	2.3%

However if we compare the loss obtained from the initial temperature rise for the first 15 seconds of the measurements, the difference increases as shown in Table 4.4. The more loss from measured temperature slope implies that loss occurring in stator of the machine is more than the loss division done for the model between stator and rotor since cutting effect will mostly be prominent in the stator as compared to rotor and difference between measured and simulated total iron loss has more contribution to the stator loss. Also, sampling rate of temperature measurement setup is slightly above 5 seconds, which might also affect the accuracy of measurement.

Table 4.4: Loss input to COMSOL model vs loss from measured temp. slope

Voltage	Stator Iron loss	Loss from simulated temperature	Loss from measured temperature	Error
$400V$	$281W$	$272W$	$292W$	3.7%
$300V$	$160W$	$159W$	$183W$	12.5%
$200V$	$85W$	$83W$	$95W$	10.5%

5   Conclusions

In this thesis work, the cage induction motor with blocked rotor test has been modelled to compute the iron losses and these losses are used in 3D thermal modelling of the machine.

In the electromagnetic modelling of the machine, the stator and rotor losses have been computed separately by calculating the hysteresis, eddy current and excess loss on the basis of their respective loss coefficient which gave a pretty good idea about the contribution factor of stator and rotor loss to the total iron loss since from the measurement, we get only the total iron loss by subtracting the copper loss from the total loss. However, the simulated iron loss lag behind the measured iron loss by some value which can be improved by including the cutting effect and better modelling techniques.

In the thermal modelling of the machine, the losses computed in the electromagnetic model are put as source in stator, rotor and winding of the machine. The symmetry of the motor geometry has been used to model $1/8^{th}$ of the total geometry to minimize the computation effort. Material properties such as thermal conductivity, effective density, specific heat capacity of the rotor and stator were computed with fairly good estimation. Convective boundary for natural convection are defined in great detail to make the model as close to actual measurement conditions as possible. The measurement is done using PT100 sensors installed in the stator and end winding of the machine and a comparative analysis of the simulated and measured data of temperature shows quite good accuracy.

The objectives of the work are achieved with fair accuracy, however there were some limitations faced during measurement of the machine which can improved in the future work. The sampling time of the temperature measurement setup was quite big to accurately compute the loss from initial rate of rise of temperature by inverse thermal technique. There were no sensors installed in the rotor of the machine, if some measurement data of temperature from the rotor is available, it will greatly enhance the accuracy of the thermal modelling. Since all the tests and simulation were done with locked rotor test, in future, this work can be extended to the fully operated machine with different loading conditions to observe the thermal profile of the motor.

References

[1] J. Pyrhonen, T. Jokinen, and V. Hrabovcova, *Design of rotating electrical machines.* John Wiley & Sons, 2013.

[2] P. C. Sen, *Principles of electric machines and power electronics.* John Wiley & Sons, 2007.

[3] D. C. Jiles and D. L. Atherton, "Theory of ferromagnetic hysteresis," *Journal of magnetism and magnetic materials*, vol. 61, no. 1-2, pp. 48–60, 1986.

[4] J. W. Macki, P. Nistri, and P. Zecca, "Mathematical models for hysteresis," *SIAM review*, vol. 35, no. 1, pp. 94–123, 1993.

[5] C. Graham Jr, "Physical origin of losses in conducting ferromagnetic materials," *Journal of Applied Physics*, vol. 53, no. 11, pp. 8276–8280, 1982.

[6] G. Bertotti, "General properties of power losses in soft ferromagnetic materials," *IEEE Transactions on magnetics*, vol. 24, no. 1, pp. 621–630, 1988.

[7] S. Kocman, P. Pečínka, and T. Hrubỳ, "Induction motor modeling using comsol multiphysics," in *International Scientific Conference on Electric Power Engineering (EPE), 2016 17th*, pp. 1–5, IEEE, 2016.

[8] M. Bose, A. Bhattacharjee, and R. Sudha, "Calculation of induction motor model parameters using finite element method," *International Journal of Soft Computing and Engineering (IJSCE)*, vol. 2, no. 3, pp. 41–43, 2012.

[9] L. Yan-ping, L. Jin-peng, and C. Jing, "Calculation of iron loss and stray losses for high-voltage induction motor using time-stepping finite element method," in *International Conference on Mechanic Automation and Control Engineering (MACE), 2010*, pp. 4081–4084, IEEE, 2010.

[10] I. Daut, K. Anayet, N. Gomesh, M. Asri, M. Muzhar, *et al.*, "Core loss measurements of three phase ac induction motor," in *4th International Power Engineering and Optimization Conference (PEOCO), 2010*, pp. 78–81, IEEE, 2010.

[11] A. Moses, "Importance of rotational losses in rotating machines and transformers," *Journal of Materials Engineering and Performance*, vol. 1, no. 2, pp. 235–244, 1992.

[12] M. al Qubeissi, "Proposing a numerical solution for the 3d heat conduction equation," in *Modelling Symposium (AMS), 2012 Sixth Asia*, pp. 144–149, IEEE, 2012.

[13] T. L. Bergman, F. P. Incropera, D. P. DeWitt, and A. S. Lavine, *Fundamentals of heat and mass transfer.* John Wiley & Sons, 2011.

[14] D. Gerling and G. Dajaku, "Novel lumped-parameter thermal model for electrical systems," in *European Conference on Power Electronics and Applications, 2005*, pp. 10–pp, IEEE, 2005.

[15] P. Mellor, D. Roberts, and D. Turner, "Lumped parameter thermal model for electrical machines of tefc design," in *IEE Proceedings B-Electric Power Applications*, vol. 138, pp. 205–218, IET, 1991.

[16] G. G. Guemo, P. Chantrenne, and J. Jac, "Parameter identification of a lumped parameter thermal model for a permanent magnet synchronous machine," in *2013 IEEE International Electric Machines & Drives Conference (IEMDC),*, pp. 1316–1320, IEEE, 2013.

[17] W. Wu, J. B. Dunlop, S. J. Collocott, and B. A. Kalan, "Design optimization of a switched reluctance motor by electromagnetic and thermal finite-element analysis," *IEEE Transactions on Magnetics*, vol. 39, no. 5, pp. 3334–3336, 2003.

[18] B. Funieru and A. Binder, "Thermal design of a permanent magnet motor used for gearless railway traction," in *34th Annual Conference of IEEE on Industrial Electronics, 2008. IECON 2008.*, pp. 2061–2066, IEEE, 2008.

[19] Y. Xie, C. Gu, and L. Wang, "There-dimensional temperature estimation of squirrel-cage induction motor using finite element method," in *2011 International Conference on Electrical Machines and Systems (ICEMS),*, pp. 1–5, IEEE, 2011.

[20] F. JinXin, Z. ChengNing, W. ZhiFu, and E. Strangas, "Thermal analysis of water cooled surface mount permanent magnet electric motor for electric vehicle," in *2010 International Conference on Electrical Machines and Systems (ICEMS)*, pp. 1024–1028, IEEE, 2010.

[21] J. Dong, Y. Huang, L. Jin, H. Lin, and H. Yang, "Thermal optimization of a high-speed permanent magnet motor," *IEEE Transactions on Magnetics*, vol. 50, no. 2, pp. 749–752, 2014.

[22] M. J. Colaço, H. R. Orlande, and G. S. Dulikravich, "Inverse and optimization problems in heat transfer," *Journal of the Brazilian Society of Mechanical Sciences and Engineering*, vol. 28, no. 1, pp. 1–24, 2006.

[23] A. Gilbert, "A method of measuring loss distribution in electrical machines," *Proceedings of the IEE-Part A: Power Engineering*, vol. 108, no. 39, pp. 239–244, 1961.

[24] A. Krings, S. Nategh, O. Wallmark, and J. Soulard, "Local iron loss identification by thermal measurements on an outer-rotor permanent magnet synchronous machine," in *15th International Conference on Electrical Machines and Systems, ICEMS 2012; Sapporo; 21 October 2012 through 24 October 2012*, p. 6401970, Institution of Electrical Engineers of Japan (IEEJ), 2012.

[25] H. D. Baehr and K. Stephan, "Heat conduction and mass diffusion," in *Heat and Mass Transfer*, pp. 107–273, Springer, 2011.

[26] X. Cai, M. Cheng, S. Zhu, and J. Zhang, "Thermal modeling of flux-switching permanent-magnet machines considering anisotropic conductivity and thermal contact resistance," *IEEE Transactions on Industrial Electronics*, vol. 63, no. 6, pp. 3355–3365, 2016.

[27] D. Staton, A. Boglietti, and A. Cavagnino, "Solving the more difficult aspects of electric motor thermal analysis in small and medium size industrial induction motors," *IEEE Transactions on Energy Conversion*, vol. 20, no. 3, pp. 620–628, 2005.

[28] A. Boglietti, A. Cavagnino, M. Parvis, and A. Vallan, "Evaluation of radiation thermal resistances in industrial motors," *IEEE Transactions on Industry Applications*, vol. 42, no. 3, pp. 688–693, 2006.

[29] S. Nategh, A. Krings, O. Wallmark, and M. Leksell, "Evaluation of impregnation materials for thermal management of liquid-cooled electric machines," *IEEE Transactions on Industrial Electronics*, vol. 61, no. 11, pp. 5956–5965, 2014.

[30] H. Vansompel, A. Yarantseva, P. Sergeant, and G. Crevecoeur, "An inverse thermal modeling approach for thermal parameter and loss identification in an axial flux permanent magnet machine," *IEEE Transactions on Industrial Electronics*, vol. 66, no. 3, pp. 1727–1735, 2019.

[31] "M400 50a datasheet." https://cogent-power.com/cms-data/downloads/m400-50a.pdf. Accessed: 2019-02-30.

[32] D. M. Ionel, M. Popescu, S. J. Dellinger, T. Miller, R. J. Heideman, and M. I. McGilp, "On the variation with flux and frequency of the core loss coefficients in electrical machines," *IEEE transactions on industry applications*, vol. 42, no. 3, pp. 658–667, 2006.

[33] L. Siesing, A. Reinap, and M. Andersson, "Thermal properties on high fill factor electrical windings: Infiltrated vs non infiltrated," in *2014 International Conference on Electrical Machines (ICEM)*, pp. 2218–2223, IEEE, 2014.

[34] A. Hemeida, *Electromagnetic and thermal design of axial flux permanent magnet synchronous machines*. PhD thesis, Ghent University, 2017.

...